

**THE INFLUENCE OF CELLULOSE NANOCRYSTALS ON  
PERFORMANCE AND TRANSPORT PROPERTIES OF CEMENTITIOUS  
MATERIALS AND GYPSUM**

by

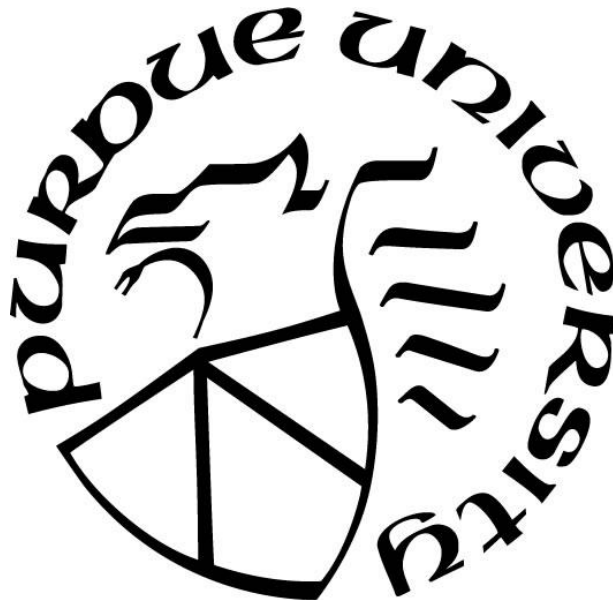
**Anthony Paul Becerril**

**A Thesis**

*Submitted to the Faculty of Purdue University*

*In Partial Fulfillment of the Requirements for the degree of*

**Master of Science in Materials Engineering**



School of Materials Engineering

West Lafayette, Indiana

December 2020

**THE PURDUE UNIVERSITY GRADUATE SCHOOL**  
**STATEMENT OF COMMITTEE APPROVAL**

**Dr. Jeffrey Youngblood, Chair**

School of Materials Engineering

**Dr. Carlos Martinez**

School of Materials Engineering

**Dr. Kendra Erk**

School of Materials Engineering

**Dr. Jan Olek**

School of Civil Engineering

**Approved by:**

Dr. David Bahr

Head of Materials Engineering Graduate Program

*To my parents, Higinio Becerril and Alma Becerril Piña, their respective family namesakes, and to the following departed family members who could not celebrate with me yet are honored with my accomplishment:*

*My son, LukaTony James Becerril,*

*My uncle, Alfredo Becerril,*

*My grandparents, 'Lela' and 'Lelo' Piña*

*My great grandparents, Mama Chavela y Papa Manuel*

*My grandpa, Higinio Becerril*

*may they rest in peace.*

## ACKNOWLEDGMENTS

First and foremost, I want to thank my advisor Dr. Jeffrey Youngblood for his knowledge and guidance. Without your honest support, patience, and passion, this thesis would not be possible. I appreciate your investment in me and my development as a researcher.

I would also like to thank Dr. Carlos Martinez, Dr. Kendra Erk, and Dr. Jan Olek for their service as my committee members. All your feedback and teachings were beneficial and appreciated.

I would like to thank my colleagues and friends as follows: Sami M. El Awad Azrak, Ana Maria Ulloa Gomez, Jose Fernando Waimin, Juan Carlos Verduzco, Alfredo Ocegueda, Mohamadreza Moini, Alejandro Alcaráz, Lysandra Perez, Tiffany Montoya, and Val Zayden Schull. Because of your time and attention, I was able to have a great graduate school experience.

A special thanks to Purdue University and the Materials Engineering Department for accepting me to take on this experience. Also, a special thanks to Oregon State University and their partnering Civil Engineering Graduate team, Dr. Jason Weiss, Yvette Valadez, Rita Maria Ghantous, and various others. I also want to thank the Dr. Youngblood research group and the Civil Engineering Department Pankow Laboratory for their assistance through my time at Purdue University.

I also want to thank the Purdue University Latino Cultural Center and their empowering staff for accepting me into their family, providing a home away from home, and nurturing me as a student and leader.

A special dedication goes out to Kobe Bryant, may he rest in peace, for he is an influence on how and why I approach challenges in life.

Lastly, I want to thank my family and best friends for the unconditional support and love in my pursuit for bettering myself as a student, engineer, and human being. Your belief in me is what has fueled me to take on my challenges whole-heartedly.

# TABLE OF CONTENTS

LIST OF TABLES .....	7
LIST OF FIGURES .....	8
ABSTRACT .....	11
1. INTRODUCTION .....	12
1.1 Background.....	12
1.2 Motivation .....	13
1.3 Objectives .....	13
1.4 Organization .....	14
2. LITERATURE REVIEW .....	15
2.1 Theoretical Background .....	15
2.1.1 Cement.....	15
2.1.2 Gypsum .....	18
2.1.3 Concrete Quality, Durability, and Transport Properties.....	20
2.1.4 Cellulose Nanocrystals .....	22
2.1.5 Cellulose Nanocrystals Cement.....	24
2.1.6 Conclusion.....	26
2.2 Test Methods .....	26
2.2.1 Concrete Resistivity .....	26
2.2.2 Rapid Chloride Permeability Test (RCPT) .....	28
2.2.3 Formation Factor .....	30
2.2.4 Mechanical Testing .....	32
2.2.5 Thermogravimetric Analysis.....	33
2.3 Conclusion .....	34
3. ASSESSING THE EFFECT OF CELLULOSE NANOCRYSTALS ON CEMENT'S RESISTANCE TO CHLORIDE INGRESS USING THE FORMATION FACTOR.....	35
3.1 Introduction .....	35
3.2 Materials .....	35
3.2.1 Sample Preparation.....	37
3.3 Methods .....	39

3.3.1	Uniaxial Resistance and Formation Factor .....	39
3.3.2	Chloride Ingress .....	41
3.4	Results and Discussion .....	42
3.4.1	Formation Factor .....	42
3.4.2	Chloride Ingress .....	43
3.5	Conclusions .....	48
4.	THE INFLUENCE OF CELLULOSE NANOCRYSTALS AND NANOFIBRILS ON GYPSUM MECHANICAL PROPERTIES AND THERMAL ANALYSIS.....	49
4.1	Introduction .....	49
4.2	Materials .....	49
4.2.1	Sample Preparation.....	51
4.3	Methods .....	51
4.3.1	Compressive Strength.....	51
4.3.2	Thermogravimetric Analysis (TGA).....	52
4.4	Results and Discussion .....	53
4.4.1	Compressive Strength.....	53
4.4.2	Thermogravimetric Analysis (TGA).....	56
4.5	Conclusions .....	59
5.	CONCLUSION.....	60
5.1	Summary.....	60
5.2	Conclusions .....	60
5.3	Future Work.....	62
	APPENDIX A: NOMENCLATURE.....	63
	APPENDIX B: ACRONYMS .....	66
	REFERENCES .....	68

## LIST OF TABLES

Table 1. Cement composition analysis by mass percentage. ....	36
Table 2. Characteristics of cellulose nanocrystals used. ....	37
Table 3. Mix design test matrix .....	38
Table 4. CNC cement estimated time to corrosion initiation for moderate chloride exposure (early and late ages).....	43
Table 5. USG No.1 pottery plaster typical physical properties .....	49
Table 6. Characteristics of cellulose nanomaterials (CNMs) used .....	50
Table 7. Cellulose-gypsum composite mix design profiles .....	51

## LIST OF FIGURES

Figure 1. Cement production process <sup>14</sup> .....	15
Figure 2. Cement notation and reaction summary .....	16
Figure 3. Schematic of cement hydration reaction <sup>12</sup> .....	16
Figure 4. Rate of heat evolution over time for cement <sup>14</sup> .....	17
Figure 6. Crystal lattices of (a) gypsum, (b) hemihydrate, and (c) anhydrite <sup>23</sup> .....	18
Figure 5. Reactions of calcium sulphate and its hydrates reactions <sup>22</sup> .....	18
Figure 7. Gypsum schematic during cement hydration <sup>14</sup> .....	19
Figure 8. Estimated 2015 use of portland cement in the United States <sup>12</sup> .....	20
Figure 9. Exposure Categories for Durable Concrete (Adapted from ACI 318) <sup>3</sup> .....	20
Figure 10 Visualization of pore types <sup>33</sup> .....	22
Figure 11. Concrete pore size range <sup>34</sup> .....	22
Figure 12. Table comparison of cellulose material properties <sup>11</sup> .....	22
Figure 13. Schematic of: (a) single cellulose chain repeat unit (b) idealized cellulose microfibril demonstrating crystalline and amorphous regions (c) cellulose nanocrystals after extraction <sup>4</sup> ...	23
Figure 14. TEM image comparison of cellulose nanocrystals (left) and nanofibrils (right) .....	23
Figure 16. CNC cement B3B flexural strength and DOH relationship <sup>41</sup> .....	25
Figure 15. An illustration of the hydration products forming around the cement grain from the age of 0–48 h in the (a) plain cement and (b) cement with CNCs on a portion of the cement particle showing SCD <sup>41</sup> .....	25
Figure 17. Two-point uniaxial method for measuring electrical resistivity <sup>28</sup> .....	27
Figure 18. Performance limits from RCPT with equivalent resistivity values <sup>49</sup> .....	29
Figure 19. AASHTO T277 / ASTM C1202 RCPT setup <sup>48</sup> .....	29
Figure 20. Correlation between RCPT and resistivity <sup>49</sup> .....	30
Figure 21. Correlation between RCPT and formation factor <sup>56</sup> .....	31
Figure 22. Schematic of splitting tensile test <sup>62</sup> .....	32
Figure 23. Concrete flexural strength setup <sup>60</sup> .....	32
Figure 24. Concrete cylinder tested in compression <sup>3</sup> .....	32
Figure 26. Cellulose-gypsum composite TGA curve (green) and DTG curve (blue) .....	33

Figure 25. Thermogravimetric analyzer furnace setup. ....	33
Figure 27. Uniaxial resistance equipment configuration <sup>67</sup> .....	39
Figure 28. Resistance measurements setup: (1) sample and sponges (2) top sponge (3) bottom sponge .....	40
Figure 29. Sample preparation summary .....	41
Figure 30. FF1 vs time (Type I/II, 0.3 w/c, 0.2% CNC).....	44
Figure 31. FF2 vs time (Type I/II, 0.35 w/c, 0.2% CNC).....	44
Figure 32. FF3 vs time (Type IIIA, 0.35 w/c, 0.2% CNC).....	44
Figure 33. FF4 vs time (Type IIIB, 0.35 w/c, 0.2% CNC).....	44
Figure 34. FF5 vs time (Type V, 0.3 w/c, 0.2% CNC).....	44
Figure 35. FF6 vs time (Type V, 0.35 w/c, 0.2% CNC).....	44
Figure 36. FF1 vs time (Type I/II, 0.3 w/c, 0.5% CNC).....	45
Figure 37. FF2 vs time (Type I/II, 0.35 w/c, 0.5% CNC).....	45
Figure 38. FF3 vs time (Type IIIA, 0.35 w/c, 0.5% CNC).....	45
Figure 39. FF4 vs time (Type IIIB, 0.35 w/c, 0.5% CNC).....	45
Figure 40. FF5 vs time (Type V, 0.3 w/c, 0.5% CNC).....	45
Figure 41. FF6 vs time (Type V, 0.35 w/c, 0.5% CNC).....	45
Figure 42. FF1 vs CNC concentration (Type I/II, 0.3 w/c, early age).....	46
Figure 43. FF2 vs CNC concentration (Type I/II, 0.35 w/c, early age).....	46
Figure 44. FF3 vs CNC concentration (Type IIIA, 0.35 w/c, early age) .....	46
Figure 45. FF4 vs CNC concentration (Type IIIB, 0.35 w/c, early age) .....	46
Figure 46. FF5 vs CNC concentration (Type V, 0.3 w/c, early age) .....	46
Figure 47. FF6 vs CNC concentration (Type V, 0.35 w/c, early age) .....	46
Figure 48. FF1 vs CNC concentration (Type I/II, 0.35 w/c, late age) .....	47
Figure 49. FF2 vs CNC concentration (Type I/II, 0.3 w/c, late age) .....	47
Figure 50. FF3 vs CNC concentration (Type IIIA, 0.35 w/c, late age) .....	47
Figure 51. FF4 vs CNC concentration (Type IIIB, 0.35 w/c, late age) .....	47
Figure 52. FF5 vs CNC concentration (Type V, 0.3 w/c, late age) .....	47
Figure 53. FF6 vs CNC concentration (Type V, 0.35 w/c, late age) .....	47

Figure 54. Cellulose-gypsum composite DTG curve comparison with a crucible (black) and without (blue).....	52
Figure 55. DTG curves: original (black), deconvolved 1st water loss (blue), deconvolved 2nd water loss (green), deconvolved total loss (red) .....	52
Figure 56. Compressive strength for cellulose-gypsum composites across three w/b ratios.....	55
Figure 57. Compressive strength for cellulose-gypsum composites with 1:1.5 b/w ratio .....	55
Figure 58. Compressive strength for cellulose-gypsum composites with 1:2 w/b ratio.....	55
Figure 59. Compressive strength for cellulose-gypsum composites with 1:2.5 w/b ratio .....	55
Figure 60. Binder/water ratio dependence for the following concentrations: 0% (REF), 0.1% CNC, 0.33% CNC, 1% CNC, 0.1% CNF, 0.33% CNF .....	55
Figure 61. Compressive Strength CNC/CNF concentration dependence for all profiles except profile no. 5 (CNC 3.33wt%, 1:2.5 w/b ratio) .....	55
Figure 62. Cellulose-gypsum composite DTG curves for all 1:1.5 w/b ratio profiles (1-7 legend top to bottom).....	57
Figure 63. Cellulose-gypsum composite DTG curves for all 1:2 w/b ratio profiles (8-13 legend top to bottom).....	57
Figure 64. Cellulose-gypsum composite DTG curves for all 1:2.5 w/b ratio profiles (14-20 legend top to bottom).....	57
Figure 65. Cellulose-gypsum composite total mass losses.....	57
Figure 66. Deconvolved cellulose-gypsum composite DTG curves for all 1:1.5 w/b ratio profiles .....	58
Figure 67. Deconvolved total cellulose-gypsum composite DTG curves for all 1:1.5 w/b ratio profiles .....	58
Figure 68. Deconvolved cellulose-gypsum composite DTG curves for all 1:2 w/b ratio profiles .....	58
Figure 69. Deconvolved total cellulose-gypsum composite DTG curves for all 1:2 w/b ratio profiles .....	58
Figure 70. Deconvolved cellulose-gypsum composite DTG curves for all 1:2.5 w/b ratio profiles .....	58
Figure 71. Deconvolved total cellulose-gypsum composite DTG curves for all 1:2.5 w/b ratio profiles .....	58

## ABSTRACT

Concrete is in everyday life such as parking lots, buildings, bridges, and more. To keep concrete and its constituents together, binders such as cement are used. Cement's production process is responsible for 8% of global carbon dioxide emissions as of 2018. With global warming being a severe global issue, the challenge of reducing cement carbon dioxide emissions can be greatly beneficial with even slight improvements. Various solutions to this challenge have developed over the years in the form of processing efficiency, material substitution, or material additives. Of the additives for cement and concrete that have been ventured, nanomaterials have had a strong development in recent years. Specifically, cellulose nanomaterials in the form of nanocrystals, nanofibrils, and more have demonstrated great improvement in cement's performance resulting in a reduction in cement produced and reduction in emissions. This study expands on the knowledge of cellulose nanocrystals as an additive for cement using the formation factor methodology. Formation factor is a resistivity ratio of the specimen and pore solution that can be used in correlation to the diffusion of chloride ions through the use of the Nernst-Einstein equation. This study also investigates the effect that cellulose nanomaterials have on the mechanical properties and thermogravimetric analysis of gypsum, a material commonly used in cement production that delays the hardening of cement.

# 1. INTRODUCTION

## 1.1 Background

Concrete is one of the longest existing technologies and is used in many construction products and infrastructures such as roads, parking lots, buildings, and more. Not to be confused with concrete, cement is the main binder, or glue, used to keep all the ingredients in concrete together. As of 2018, cement production is responsible for 8% of global carbon dioxide (CO<sub>2</sub>) emissions<sup>1</sup>. Cement production has not decreased over the years resulting in a constant contribution to global warming. The excess CO<sub>2</sub> in the atmosphere is leading to potential ecological, physical, and health impacts<sup>2</sup>. This raises concern and demands improvement in concrete sustainability, the ability to economically uphold engineering goals whilst preserving the existing ecosystem with no hard or resource depletion<sup>3</sup>. To address this, concrete additives such as supplementary cementitious materials (SCM), chemical admixtures, and nanomaterials have been widely used to improve concrete performance such as durability. Of the many nanomaterials used in cement and concrete, cellulose nanomaterials (CNMs) provide a renewable, biodegradable resource while also improving environmental, economic, and health impacts<sup>4</sup>. Specifically, cellulose nanocrystals (CNCs) as an additive for cement has demonstrated improved performance through improved flexural strength, microstructure enhancement, and an increase in the degree of hydration (DOH)<sup>5</sup>. To determine the quality of cement or concrete, it is evaluated by meeting specifications or standards of mix design and structural performance requirements. These standards and requirements analyze the main parameters of cement and concrete in its wet (freshly mixed) and dry (hardened) forms that are important for longevity that safety and sustainability demand<sup>6</sup>. Durability, one of the many important parameters for hardened concrete quality, is tested with methods such as mechanical strength testing and rapid chloride permeability test (RCPT) which are considered destructive testing due to how the sample is unusable for further testing<sup>7</sup>. Alternatively, non-destructive testing (NDT) methods, such as resistivity measurements and ultrasonic pulse velocity, evaluate concrete without harm or impairment for future testing<sup>7,8</sup>. Formation factor is a developing NDT method that has potential in replacing the existing RCPT as an equivalence between the two methods has been shown<sup>9</sup>. Formation factor testing in comparison to RCPT is more efficient in directly relating measured concrete transport properties

to the long-term durability performance of concrete structures<sup>9</sup>. In this work, the effect of cellulose nanocrystals on cement's resistance to chloride ingress will be discussed using formation factor methodology. Additionally, the influence of cellulose nanocrystals and nanofibrils on gypsum's thermal analysis and mechanical properties.

## **1.2 Motivation**

Cement production is responsible for global carbon dioxide emissions and has been approached for reduction in various ways including but not limited to partial replacement of cement via supplementary cementitious materials (SCMs) or alternative cement materials for total replacement of cement such as geopolymers<sup>1</sup>. Another approach avoiding replacement is through use of additives, substances added to improve upon certain material properties. Additives range from chemical admixtures to SCMs to nanomaterials and have been widely used due to improvement in performance<sup>10</sup>. Although a relatively new nanomaterial in cement and concrete applications compared to the likes of nanosilica, cellulose nanomaterials (CNMs) have been a great addition due to being an abundant, renewable, and sustainable material that can improve performance while reducing environmental impacts<sup>4,11</sup>. The vision here is to further develop the knowledge base on CNM and cementitious material interactions such that implementation of CNMs into existing industry cement production processes can exist and start contributing towards resolving global warming.

## **1.3 Objectives**

The key objective is to expand on the existing CNM and cementitious material interactions knowledge. Specific to cellulose nanocrystals (CNCs), the objective is to determine the effects of CNC concentration and surface chemistry on the cement structure, chemistry, and mechanical strength properties. There is a need to determine the effects of CNC on the adsorption and diffusive pathways of water<sup>4</sup>. The surface chemistry of CNCs impacts the interactions with the pore solution, cement particles, and hydration product, as the full nature of these interactions is currently unknown. Structure, chemistry, and durability properties within CNC cement will be studied with a focus on correlation to cement type, CNC concentration, and CNC chemistry.

## 1.4 Organization

This thesis has the following organization:

**INTRODUCTION** – This chapter introduces the big picture and importance of this study’s research efforts through a brief background, motivation, and research objectives.

**LITERATURE REVIEW** – This chapter establishes a knowledge base on the materials (cement, cellulose nanocrystals, and cellulose nanofibrils) and methodology (formation factor, thermogravimetric analysis, and mechanical testing) used in the study.

**ASSESSING THE EFFECT OF CELLULOSE NANOCRYSTALS ON CEMENT’S RESISTANCE TO CHLORIDE INGRESS USING THE FORMATION FACTOR** – This chapter will discuss in detail the experiment completed regarding the effect CNCs have on cement’s resistance to chloride ingress through use of a developing NDT method, formation factor.

**THE INFLUENCE OF CELLULOSE NANOCRYSTALS AND NANOFIBRILS ON GYPSUM MECHANICAL PROPERTIES AND THERMAL ANALYSIS** – This chapter will discuss in detail the experiment completed regarding how CNMs affect gypsum’s mechanical properties and a thermal analysis.

**CONCLUSION** – This chapter will close out the document with a summary of the learning points and future work.

.

## 2. LITERATURE REVIEW

### 2.1 Theoretical Background

#### 2.1.1 Cement

Concrete is a durable material by being an economical, cost-effective solution that consumes minimal materials, energy, and other resources for construction, maintenance, and rehabilitation over its lifetime<sup>3</sup>. In common concrete mixes, cement is the main binder that keeps all the ingredients together. While concrete that uses cement is durable, the need for improving its sustainability is critical due to 8% of global carbon dioxide (CO<sub>2</sub>) emissions rooting from annual cement production<sup>1,12</sup>. Ordinary portland cement (OPC) is the most common and generic type of cement manufactured and is maintained via American Society for Testing and Materials (ASTM) C150 and American Association of State Highway and Transportation Officials (AASHTO) M85 specifications<sup>3</sup>. OPC is a hydraulic cement composed primarily of calcium silicates meaning that it will set and harden upon reacting chemically with water<sup>3</sup>. Cement production starts with the raw materials of calcium, iron, silica, alumina, and sulfate are processed through a roller mill to crush, grind and dry them into a blended powder<sup>3,13</sup>. This powder passes through a

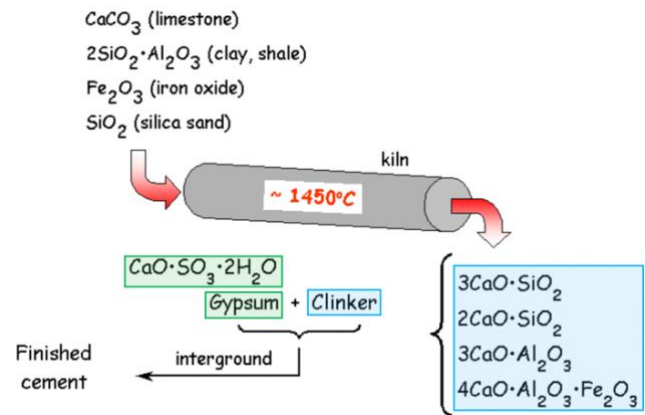


Figure 1. Cement production process<sup>14</sup>

kiln and is heated to approximately 1450°C to form the predominant four hydraulic compounds known as clinker as shown in Figure 1: tricalcium silicate (C<sub>3</sub>S) (also known as alite); dicalcium silicate (C<sub>2</sub>S) (also known as belite); tricalcium aluminate (C<sub>3</sub>A), and tetracalcium aluminoferrite (C<sub>4</sub>AF)<sup>13,14</sup>. Cement notation and compounds are labeled using cement chemist's notation as summarized in Figure 2. Cement is typically 52% C<sub>3</sub>S, 22% C<sub>2</sub>S, 7% C<sub>3</sub>A, and 11% C<sub>4</sub>AF<sup>15</sup>. During this heating stage, CO<sub>2</sub> is a by-product contributing to global warming. After the clinker is

Raw Materials		
Name	Oxide	Abbrev
Lime	CaO	C
Silica	SiO <sub>2</sub>	S
Alumina	Al <sub>2</sub> O <sub>3</sub>	A
Ferric Oxide	Fe <sub>2</sub> O <sub>3</sub>	F
Magnesium Oxide	MgO	M
Sulfur Trioxide	SO <sub>3</sub>	\$
Water	H <sub>2</sub> O	H

Cement Powder		
Name	Compound	Abbrev
Alite	3CaO · SiO <sub>2</sub>	C <sub>3</sub> S
Belite	2CaO · SiO <sub>2</sub>	C <sub>2</sub> S
Tricalcium Aluminate	3CaO · Al <sub>2</sub> O <sub>3</sub>	C <sub>3</sub> A
Tetracalcium Aluminoferrite	4CaO · Al <sub>2</sub> O <sub>3</sub> · Fe <sub>2</sub> O <sub>3</sub>	C <sub>4</sub> AF
Gypsum (calcium sulfate)	CaSO <sub>4</sub> · 2H <sub>2</sub> O	C\$H <sub>2</sub>

Hydration Products		
Name	Product	Abbrev
Calcium Silicate Hydrate	C <sub>1.7-2.1</sub> S(A <sub>0.03-0.05</sub> S <sub>0.04</sub> )H <sub>x</sub>	C-S-H
Calcium Hydroxide	CaO · H <sub>2</sub> O	CH
Etringite	C <sub>6</sub> A <sub>3</sub> H <sub>32</sub>	C <sub>6</sub> A\$H <sub>32</sub>
Calcium Monosulfoaluminate	C <sub>4</sub> A\$H <sub>12</sub>	C <sub>4</sub> A\$H <sub>12</sub>
Tetracalcium Aluminate Hydrate	C <sub>4</sub> AH <sub>13</sub>	C <sub>4</sub> AH <sub>13</sub>
Calcium Aluminoferrite Hydrate	C <sub>4</sub> AFH <sub>12</sub>	C <sub>4</sub> AFH <sub>12</sub>

Figure 2. Cement notation and reaction summary

rapidly cooled, it is combined with gypsum for the final fine cement powder being ready for transport<sup>3</sup>. Gypsum, also denoted as C\$H<sub>2</sub>, is added to delay the setting cement and will be further discussed in the following section. Cement powder requires hydration in order to create adhesion. Cement hydration, an exothermic chemical reaction, occurs when water is added to cement and creates the main hydration products responsible for strength and adhesion development<sup>12,16</sup>. The hydration process, as outlined in Figure 3, starts when the manufactured, anhydrous cement is put in water and ions dissolve<sup>12</sup>. This eventually results as the main hydration products: calcium silicate hydrate (C-S-H); calcium hydroxide (CH); ettringite (C<sub>6</sub>A\$H<sub>32</sub>); and calcium monosulfoaluminate (C<sub>4</sub>A\$H<sub>12</sub>). To reach the final products, the ion dissolution creates a saturated pore solution that initiates hydration of the cement grains by forming a thin layer of C-S-H gel on cement grains surfaces and precipitates of C-S-H and CH. As time passes, the precipitates form ettringite needles as the “outer”, fibrous C-S-H and the C-S-H surrounding the cement grains thicken as the “inner” C-S-H.

The combination of the needles and shells among cement grains are what creates the binding action where C-S-H accounts for most of the strong and dense structure creation. The final hydration products typically

result in 50–60% C-S-H, 20–25% CH, and 15–20% calcium sulfoaluminates<sup>16</sup>. The cement hydration reactions are outlined below and further explanation can be found in literature:

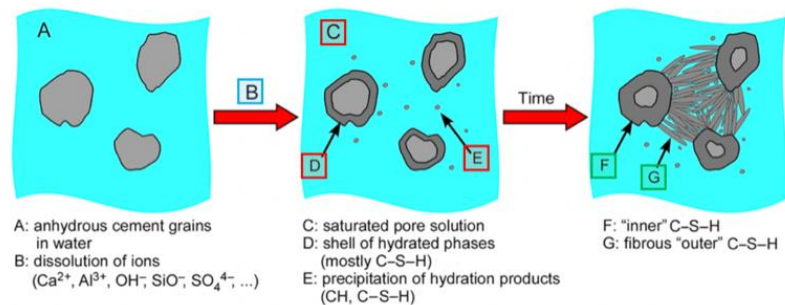
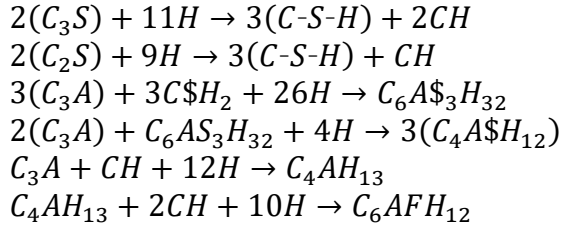


Figure 3. Schematic of cement hydration reaction<sup>12</sup>



*Equation 1.*  
*cement compound hydration reactions<sup>3</sup>*

Each compound of OPC varies in its reaction to water meaning changes in the initial compound composition affect cementing development<sup>16</sup>. This sheds light on how OPC types differ and explain why a cement with finer grains (Type III) demonstrates high early strength and a cement with low C<sub>3</sub>A (Type V) demonstrates high sulfate resistance. ASTM C150 is the standard specification for OPCs and defines various common OPC types.

Another way of looking at hydration is through the rate of heat evolution over time as demonstrated in Figure 4<sup>14</sup>. It starts with a high rate of heat evolution due to dissolution and ettringite formation. Then an induction period follows that is possible due to gypsum in cement.

After some time, cement initiates setting, and rapid formation of C-S-H and CH occurs. Setting occurs when the OPC paste stiffens and takes shape until the eventual final set where from then on cement is considered no longer workable and eventually reaches steady state rate of heat evolution. Setting is not to be confused with hardening which occurs after

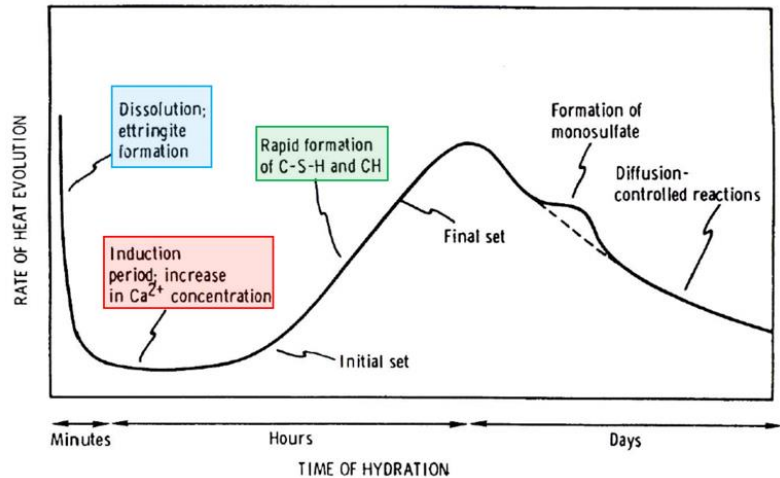


*Figure 4. Rate of heat evolution over time for cement<sup>14</sup>*

setting and accounts for strength development<sup>16</sup>. The anhydrous cement from the start doesn't fully hydrate leaving unhydrated cement grains. To measure hydration the degree of hydration (DOH) is taken and is the fraction of cement that has reacted with water whereas a DOH of 1 indicates all of the cement has reacted<sup>17</sup>. This has been measured using scanning electron microscopy (SEM) quantitative techniques, thermogravimetric analysis, isothermal calorimetry, x-ray measurements, and other techniques<sup>18,19</sup>. Cementitious materials are unique in their transformation cycle from raw

materials to hydration products. And as the binder for concrete constituents, cement has long been reliable and has improved over the years in durability, strength, and economic efficiency.

### 2.1.2 Gypsum

Ordinary portland cement (OPC) is a combination of clinker and gypsum where the addition of gypsum allows an induction period in hydration<sup>20</sup>. Gypsum, or calcium sulfate dihydrate (D) is 79.1% calcium sulfate and 20.9% water<sup>21</sup>.

Also commonly called stucco in industry, hemihydrate is added to water resulting in gypsum after setting<sup>21</sup>. When gypsum is heated, two dehydration steps occur as illustrated in Figure 6. The first step is a water mass loss of 1.5 H<sub>2</sub>O occurring between 110 and 130 °C. The second step C is a water mass loss of 0.5 H<sub>2</sub>O occurring between 150 and 200

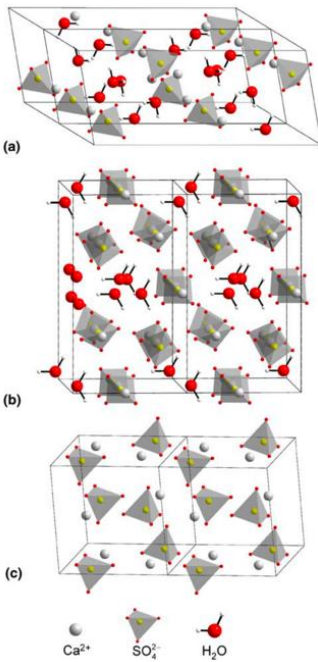
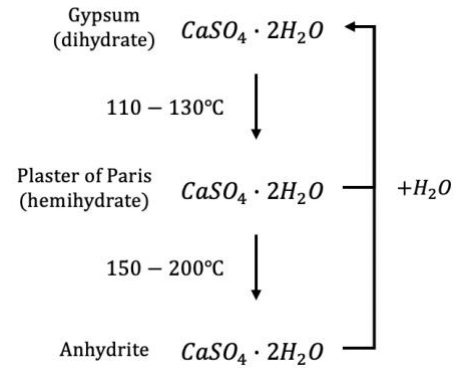
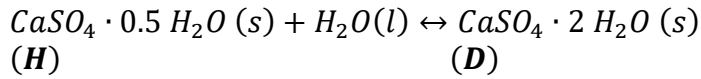


Figure 5. Crystal lattices of (a) gypsum, (b) hemihydrate, and (c) anhydrite<sup>23</sup>

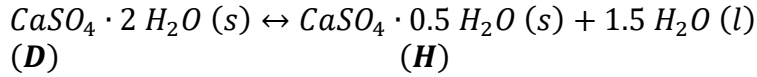
°C resulting in calcium sulfate anhydrite (A)<sup>22</sup>. Gypsum when undergoing the first

dehydration step causes rearrangement of Ca<sup>2+</sup> and SO<sub>4</sub><sup>2-</sup> ions such that water molecules are removeable during dehydration resulting in shrinkage and increased density<sup>21</sup>. Further dehydration from hemihydrate to anhydrite does not have ion movement rather repositions its crystal structure to create hexagonal canals from tetrahedral consisting of Ca<sup>2+</sup> cations and SO<sub>4</sub><sup>2-</sup> anions resulting in another decrease in density as demonstrated in Figure 5<sup>23</sup>. These dehydration steps are not naturally separate and overlap but have been separated in literature previously<sup>22</sup>. The total mass loss from both reactions is theoretically 20.9% (15.7% from the first dehydration step, 5.2% from the second) according to stoichiometry<sup>24,25</sup>. Both the temperature ranges and mass losses vary depending on the mix design and experimental setup<sup>21,22</sup>. The reactions have been outlined below:

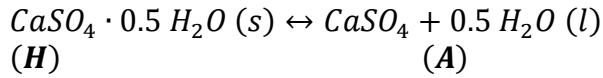
Figure 6. Reactions of calcium sulphate and its hydrates reactions<sup>22</sup>



Equation 2.  
hemihydrate to dihydrate reaction



Equation 3.  
dihydrate to hemihydrate reaction



Equation 4.  
hemihydrate to anhydrite reaction

In cement applications, gypsum is added during milling in order to delay hydration specifically by creating a reaction between gypsum and C<sub>3</sub>A that results in an ettringite coating<sup>20,23</sup>. This coating breaks over time as ettringite reacts with water and C<sub>3</sub>A but will heal the coating as long as gypsum and C<sub>3</sub>A are still available for replenishing. When gypsum and C<sub>3</sub>A are no longer creating ettringite and all the ettringite coating breaks free into monosulphoaluminate, the remaining C<sub>3</sub>A is made into tetracalcium aluminate hydrate which is then made to calcium aluminoferrite hydrate, one of the main cement hydration products<sup>20</sup>. The stages of gypsums described are illustrated in Figure 7<sup>14</sup>. Inclusion of gypsum in cement prevents hydration from occurring within 10 minutes

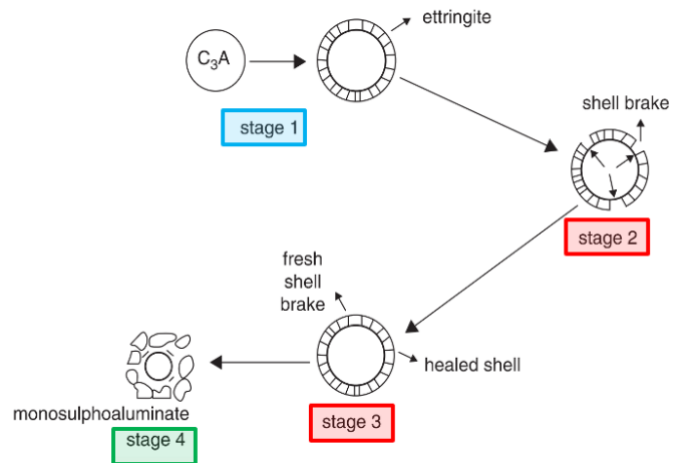


Figure 7. Gypsum schematic during cement hydration<sup>14</sup>

otherwise and allows cement to be mixed and transported to application sites without worry for setting prior to arrival<sup>26</sup>. Gypsum is an old building materials with many advantages such as easy fabrication, low price, fire resistance, sustainability, and more<sup>27</sup>. It is gypsum's chemical, thermal, and mechanical properties that play a critical role in delaying fire from spreading in building applications by absorbing energy during dehydration<sup>21</sup>.

### 2.1.3 Concrete Quality, Durability, and Transport Properties

Cementitious materials have long been reliably applied in roads, housing, parking lots, buildings and more as demonstrated in Figure 8<sup>12</sup>. Reliability depends on the quality of concrete which is well defined through requirements of two areas: freshly mixed concrete and hardened concrete<sup>3</sup>. Freshly mixed concrete looks at consistency, stability, uniformity, workability, and finishability whereas hardened concrete looks to strength, durability, appearance, and economy. Altogether, these concrete parameters must be analyzed depending on the desired engineering properties for the application<sup>12,16</sup>. Due to the numerous parameters, the focus of this study will focus on strength and durability with strength discussed in methodology. Durability is defined as the ability to resist deterioration processes and in concrete applications durability is indicated by how well the concrete performance in certain exposures<sup>3</sup>. According to the American Concrete Institute's (ACI) 318 building code requirements, exposure categories for durability are broken down into the following four categories: freezing and thawing (F), sulfate attack (S), corrosion protection of reinforcement (C), and being in contact with water (W) as illustrated below<sup>3</sup>.

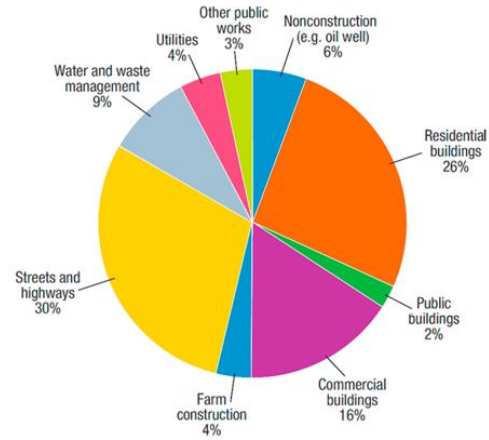


Figure 8. Estimated 2015 use of portland cement in the United States<sup>12</sup>

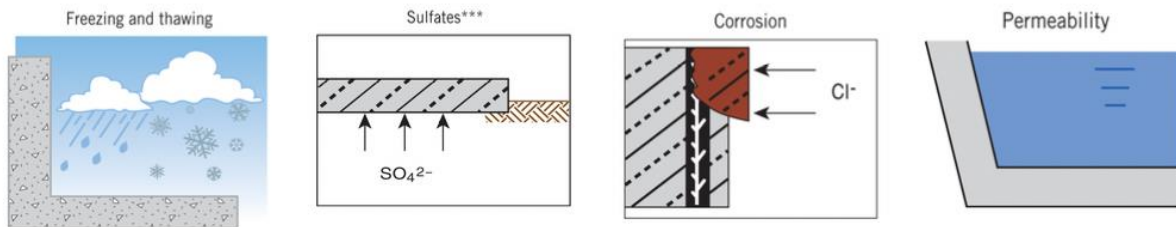


Figure 9. Exposure Categories for Durable Concrete (Adapted from ACI 318)<sup>3</sup>

Each of these categories have their own testing methods to define the class of severity levels outlined in ACI 318. For example, a parking lot that experiences winter can be within both F and C exposure categories due deicing salts (corrosion) used to thaw snow (freezing and thawing) leading to design requiring withstanding both conditions. To measure the penetration of ions,

liquids, or gases in concrete, transport mechanisms such as permeation, absorption, and diffusion are measured through performance testing of durability characteristics such as sulfate attack, frost resistance, abrasion, chloride ingress, porosity, and many more<sup>16,28</sup>. The transport properties permeability, diffusivity, and porosity alone do not define durability but are highly interconnected and in combination can help assess a concrete's durability thoroughly.

ACI 318's W exposure category is also called permeability, the property that measures fluid flow through concrete when applying pressure<sup>29</sup>. This becomes critical for applications in tunnels or dams. High permeability is desired not only for water resistance but also contributes to resisting chlorides or sulfates that dissolve in water<sup>29</sup>. A concrete structure's service life can be measured on how well it resists the diffusion of deteriorating ions. Diffusion is defined as the movement of ions such as chloride or sulfate ions in pore solution although solution flow isn't required<sup>29,30</sup>. Most commonly, chloride ingress has been estimated using methods such as Fick's second law and the Nernst-Planck equations<sup>31</sup>. Fick's second law can help determine chloride concentration in concrete depending on time exposed to a chloride concentration gradient as show in the equation below<sup>31</sup>:

$$\frac{C_{x,t} - C_0}{C_s - C_0} = \operatorname{erfc}\left(\frac{x}{2\sqrt{D_a t}}\right)$$

*Equation 5.  
Fick's Second Law<sup>31</sup>*

Where  $C_{x,t}$  is the chloride concentration at time t (seconds) at depth x (meters) (% by mass of concrete);  $C_0$  is the background chloride concentration (% by mass of concrete);  $C_s$  is the chloride concentration at the surface (% by mass of concrete);  $D_a$  is the apparent chloride diffusion coefficient ( $m^2/s$ );  $\operatorname{erfc}(y)$  is the complimentary error function of  $y$ <sup>31</sup>. This can be used to estimate the life cycle of a certain material and is commonly tested in industry with bulk diffusion tests<sup>32</sup>.

As concrete hardens, the resulting pore structure defines porosity, the volume of voids compared to the total volume<sup>33</sup>. The pores/voids can be in the form of entrapped air voids (1-4mm), entrained air (100um-1mm), capillary pores (5nm–10mm), and gel pores (2–5nm) as illustrated below<sup>33-34</sup>.

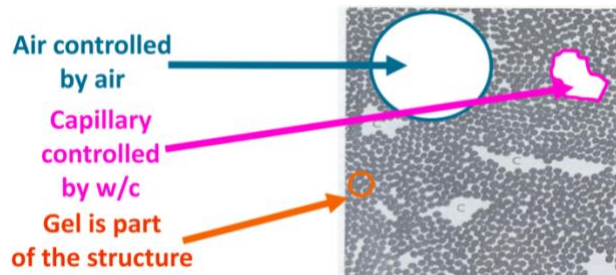


Figure 10 Visualization of pore types<sup>33</sup>

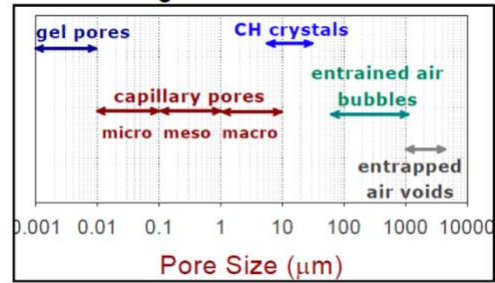


Figure 11. Concrete pore size range<sup>34</sup>

The pores not only vary in type but also in size distribution and connectivity. Porosity is highly dependent on the concrete mix design, specifically the water-to-cement (w/c) ratio. The w/c ratio defines how much water is available for cement’s hydration hence the degree of hydration<sup>34</sup>. Over time porosity generally decreases due to hydration filling pores with hydration products. A higher w/c ratio will reduce the hydration product and increase dispersion resulting in more porosity<sup>34</sup>. To avoid less durable mix designs, organizations such as the ACI and ASTM have documented requirements on High-performance concrete (HPC), a concrete designed to be more durable and strong than regular concrete using a lower w/c ratio, and numerous other concrete mix designs to control porosity through strength requirements<sup>35</sup>. The resulting pore structure is critical in defining transport properties and concrete properties such as permeability and durability<sup>34</sup>. Transport properties alone do not define concrete reliability considering the various effects environments can have on it. These transport properties help define durability but are not to be confused with strength for they are two different hardened concrete parameters that determine the quality of concrete<sup>8</sup>.

#### 2.1.4 Cellulose Nanocrystals

As stated previously, there is a need for advancing concrete’s performance and sustainability. To address this, nanomaterials such as nanosilica and carbon nanotubes (CNTs) have been used in cement and concrete research for many years. Cellulose is not only a new nanomaterial but also the most abundant

Material	Tensile strength (GPa)	Young’s modulus (GPa)	Density (g/cm <sup>3</sup> )	Tensile/ density	Modulus/ density	Thermal exp. coe. (ppm/K)
CNC	7.5	145	1.6	4.7	90.6	3-22
Glass fiber	4.8	86	2.5	1.9	34.4	13
Steel wire	4.1	207	7.8	0.5	26.5	15
Kevlar	3.8	130	1.4	2.7	92.9	-4
Graphite	21	410	2.2	9.5	186	2-6
CNT	11-73	270-970	1.0	11-73	270-970	-

Figure 12. Table comparison of cellulose material properties<sup>11</sup>

organic material in the world and a naturally hydrophilic polymer<sup>36</sup>. Cellulose as an abundant, renewable, and sustainable additive can improve cement performance while reducing

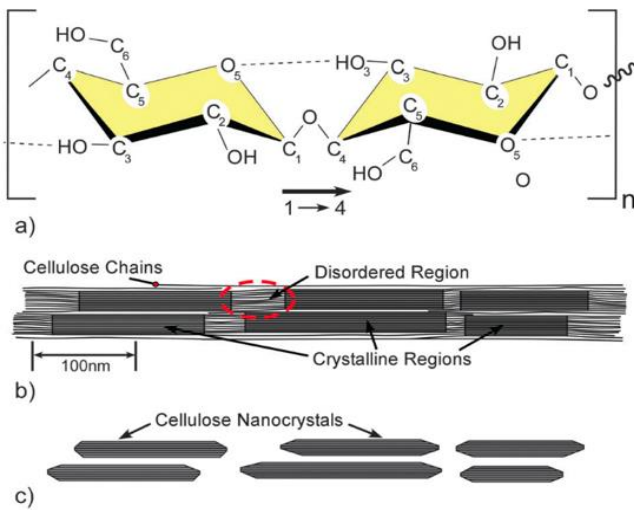


Figure 13. Schematic of: (a) single cellulose chain repeat unit (b) idealized cellulose microfibril demonstrating crystalline and amorphous regions (c) cellulose nanocrystals after extraction<sup>4</sup>

environmental impacts<sup>4,11</sup>. Cellulose nanomaterials such as cellulose nanocrystals (CNCs) and cellulose nanofibrils (CNFs) have been gaining momentum in cement research<sup>10</sup>. Among cellulose particle types, cellulose nanocrystals (CNC) is the most sought after for cement improvement<sup>37,38</sup>. This is due to CNC's unique physical properties combination of high tensile strength (7.5 GPa), high elastic modulus (145 GPa), relatively low density (1.6 g/cm<sup>3</sup>), and high aspect ratio (3–5 nm wide, 50–500 nm in length) as demonstrated in Figure 12<sup>11</sup>. To obtain CNC, it must be extracted from

cellulose microfibrils within the natural cellulose that sources from trees, plants, tunicates, algae, and bacteria<sup>4</sup>.

Cellulose microfibrils have amorphous and crystalline regions and undergo a chemical extraction such as acid hydrolysis to eliminate of the amorphous regions as illustrated in Figure 13<sup>4</sup>. The remaining crystalline regions are highly crystalline (54-88%) and are called CNCs<sup>39</sup>. CNCs are also known as whiskers or rods. CNC provide cementitious materials with superior mechanical properties (tensile strength up to 700 MPa), high water retention for internal curing (absorption capacity over 300%), and sustainability as an abundant, biodegradable, low-cost material<sup>12,40</sup>. CNF differ from CNC due to a difference in processing. Whilst CNC undergoes acid hydrolysis, CNF are obtained by mechanical treatment of cellulose. CNF's larger dimensions (10–100 nm diameter, 0.5–10um length) and lower crystallinity (51–

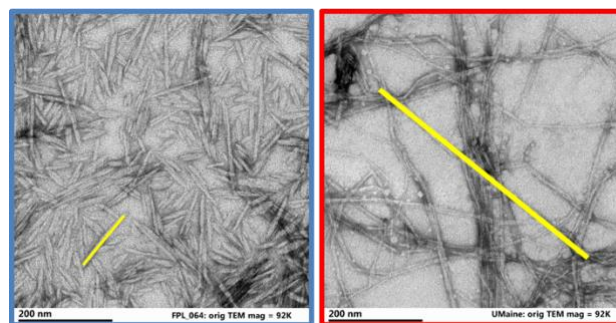


Figure 14. TEM image comparison of cellulose nanocrystals (left) and nanofibrils (right)

69%) in comparison to CNC attribute to why CNC are more transparent in suspension<sup>4,39</sup>. A comparison of the two materials is illustrated in Figure 14. Both CNC and CNF along with other forms of nanocellulose have great potential for advancing cement research to become more efficient.

### **2.1.5 Cellulose Nanocrystals Cement**

Additives when used correctly can result in superior cement with improvements in: cohesiveness, workability, temperature development, strength, permeability, and durability<sup>12</sup>. More specifically, additives for fiber reinforcement in cementitious materials have been long used due to their high aspect ratio that improve flexural strength<sup>12</sup>. Metaxa et al. found CNTs present in cement demonstrate microcrack bridging and increase flexural strength by 25%<sup>41</sup>. With CNCs being significantly smaller than most fibers mentioned, its reinforcing ability should not be defaulted to microcrack bridging<sup>41</sup>. CNCs in cement have demonstrated improved performance through increase in the degree of hydration, improved flexural strength, and microstructure enhancement<sup>5</sup>.

Cao et al. demonstrated that adding CNC to cement increases DOH which can be attributed to the two mechanisms steric stabilization and short circuit diffusion (SCD)<sup>41</sup>. While steric stabilization has been observed to disperse cement particles in water reducing admixtures (WRAs) by inhibiting coagulation, SCD diffuses water through the adsorbed CNCs. CNCs initially adhere to the cement particles and remain in the hydration product shell (i.e., the high density C-S-H), possibly forming a path to transport pore water to the inner unhydrated cement as illustrated in Figure 16<sup>41</sup>. Flores et al. demonstrated that CNC in cement show a similar effect on DOH by delaying hydration at early ages and enhancing it at later ages<sup>10</sup>. When CNC is added, there is an initial hydration delay due to CNC adsorption onto cement particles which reduce the surface area for the hydration reaction. Then at later ages, CNC adsorption improves hydration due to the proposed SCD mechanism.

CNCs and cement are distinct materials that when combined may alter the microstructure. How the CNC distributes in cement paste may drive the resulting microstructure. Cao et al. demonstrated that CNCs influence cement microstructure by decreasing porosity<sup>40</sup>. This is due to the majority of CNCs being absorbed when dispersed over the cement surface. This porosity reduction also indicates an increase in DOH. Cao et al. discovered sonication reduces large size porosity and whilst dispersing CNC well, the majority still adsorb to cement particle surfaces (94.2%–96.5%) regardless of sonication<sup>17</sup>. The interaction forces between CNC and cement favoring adsorption cause a delay in hydration. Flores et al. compared surface charge data using zeta potential measurements and the larger surface charge of CNC (-33.4 mV to cement's -10 mV) explain why adsorption onto cement particles occurs rather than agglomerating with themselves, reinforcing steric stabilization<sup>10,41</sup>. With all the CNCs covering up the cement particles, cement particles cease hydration and start

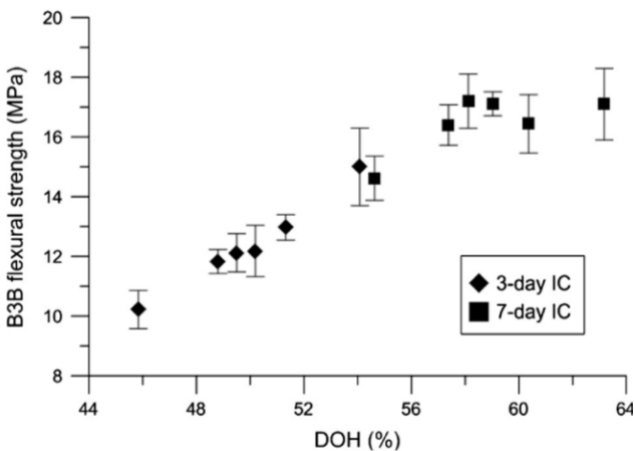


Figure 15. CNC cement B3B flexural strength and DOH relationship<sup>41</sup>

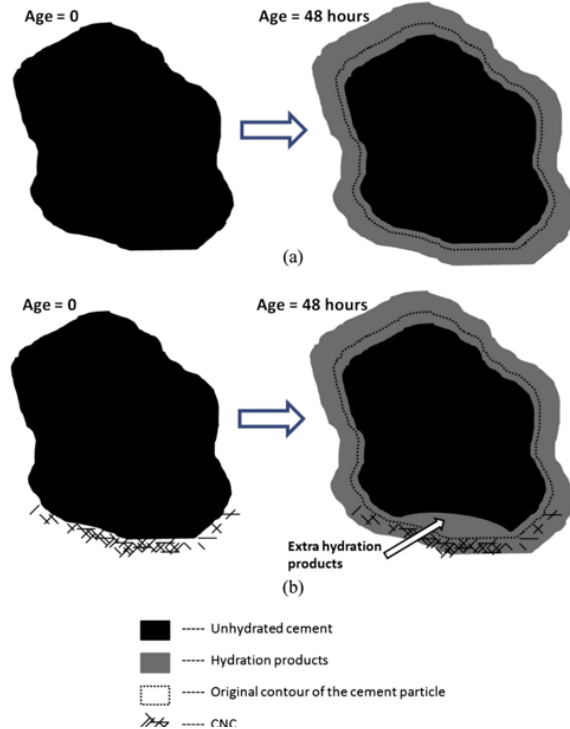


Figure 16. An illustration of the hydration products forming around the cement grain from the age of 0–48 h in the (a) plain cement and (b) cement with CNCs on a portion of the cement particle showing SCD<sup>41</sup>

back up later during SCD.

Fu et al. demonstrated that CNC at low dosages (0.2% by volume of cement) increase flexural strength up to 20% for cement Type I/II and Type V systems<sup>5</sup>. While both systems increase in flexural strength, the effectiveness of CNC depends on tricalcium aluminate content as well as having an optimum dosage in order to prevent agglomeration<sup>10</sup>. Cao et al. demonstrated that

CNCs improve cement flexural strength by 20%–30% due to its linear increase as a function DOH as illustrated in Figure 15<sup>41</sup>. Currently, CNC as an additive for cement remains mostly in the academic realm with a need to implement into industrial production. For CNC to integrate into existing cement production, CNC must be specifically tailored for its mix design's application much like cement and concrete are. To do that the interaction between cement and CNC must be further understood such that implementation is more seamless.

### **2.1.6 Conclusion**

Concrete has long been used in world construction for its reliability as a material and developing technology. What is less known is cement production's CO<sub>2</sub> emissions contributing to global warming. With a shift towards greener products, the use of sustainable and renewable materials is the solution to this problem. Additives from supplementary cementitious materials to chemical admixtures to nanomaterials have been investigated and implemented to improve cement performance. Better cement performance will reduce the demand in cement production resulting in lower CO<sub>2</sub> emissions. Cellulose nanomaterials such as CNCs and CNFs are great additives for cement performance improvement but until the knowledge of cellulose nanomaterial and cement interactions are better developed, transition from academia to industry integration in cement production will have to wait.

## **2.2 Test Methods**

### **2.2.1 Concrete Resistivity**

Electrical resistivity is standardized via the American Society for Testing and Materials (ASTM) C 1760 "Standard Test Method for Bulk Electrical Conductivity of Hardened Concrete" and the American Association of State Highway and Transportation Officials (AASHTO) TP 95-11 "Surface Resistivity Test Evaluation as an Indicator of the Chloride Permeability of Concrete," quantify concrete resistivity for indicating concrete durability but is still bridging the gap between knowledge and industry practice<sup>28</sup>. Electrical resistivity is a material property that quantifies how well a material resists electrical current. In concrete, resistivity is the ability to hold out against the transfer of ions through the microstructure<sup>28,42</sup>. Due to this, resistivity is highly dependent on the solution within the pores, the concrete microstructure (pore sizes, shapes, and tortuosity/pore

connectivity) and its degree of saturation<sup>28,43</sup>. Each experiment varies in geometry, mix design, exposure conditions, and measurement method affecting resistivity in two areas: intrinsically and through measurement setup<sup>28</sup>.

Affecting intrinsic factors that define the microstructure and pore configuration are water-to-cement ratio (w/c ratio), aggregate size and type, and curing conditions<sup>28</sup>. The w/c ratio is the main contributor to permeability since the higher the w/c, the higher the porosity, the lower the electrical resistivity resulting in a more permeable concrete<sup>28</sup>. Concrete permeability the ability to resist penetration by liquids, gases, or ions<sup>3</sup>. Although concrete permeability is dependent on the cement paste and aggregates, the paste permeability has higher importance as it surrounds and holds together all constituents and is responsible for the pore network formed<sup>3</sup>. Additionally, resistivity is affected by the degree of hydration (DOH) as further hydration typically reduces porosity and affects tortuosity<sup>28</sup>. When w/c ratio increases so does conductivity, the reciprocal of resistivity. This is due to the relative volume of interconnected pores where an increase in w/c ratio has a higher volume fraction of hydrated cement resulting in a lower resistivity<sup>28</sup>. Aggregates, apart from the type, generally read a higher resistivity compared to cement paste due to porosity reduction<sup>28</sup>. Lastly, concrete resistivity evolves over time depending on the curing regimes (temperature, humidity, sample storage). During concrete resistivity data collection, geometry, temperature, and electrode contact are critical and an example is illustrate in Figure 17<sup>28</sup>.

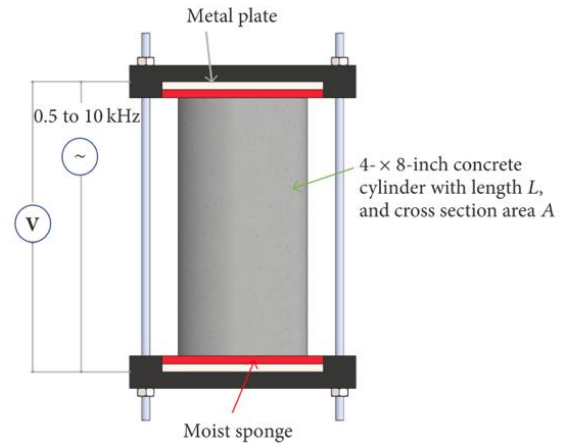


Figure 17. Two-point uniaxial method for measuring electrical resistivity<sup>28</sup>

For any electrode configurations, resistivity  $\rho$  ( $\Omega \cdot \text{m}$ ) is equal to resistance  $R$  ( $\Omega$ ) multiplied by a geometry correction factor  $k$  (unitless), dependent on sample size and electrode location, making resistivity geometry-independent:

$$\rho = R \cdot k$$

*Equation 6.  
Resistivity equation<sup>28</sup>*

During a resistance measurement, electrical current flows via dissolved charged ions into the concrete pore solution and through the microstructure<sup>28</sup>. The resulting measurement is a good indicator of the pore structure configuration because when fresh concrete sets and hardens, depercolation/disconnection of pore spaces due to hydration shrinkage increases electrical resistivity<sup>28,44</sup>. Ion diffusivity is defined as ion movement through the concrete<sup>3</sup>. This can be explained using the Nernst-Einstein equation:

$$D_i = \frac{RT\sigma_i}{Z_i^2 F^2 C_i}$$

*Equation 7.  
Ion diffusivity from the  
Nernst-Einstein equation<sup>28</sup>*

Where  $D_i$  is the diffusivity of ion  $i$  ( $\text{m}^2/\text{s}$ );  $\sigma_i$  is the partial conductivity of ion  $i$  ( $\text{S}/\text{m}$ );  $R$  is the gas constant ( $8,314 \text{ J}/\text{mol}$ );  $T$  is the absolute temperature ( $\text{K}$ );  $Z_i$  is the charge of ion  $i$ ;  $F$  is Faraday's constant ( $96500 \text{ Coulombs}/\text{mol}$ ); and  $C_i$  is the concentration of ion  $i$  ( $\text{mol}/\text{m}^3$ )<sup>28</sup>. The temperature has a significant influence on concrete resistivity due to resistivity's dependency on ions flow affected by temperature change; higher temperatures move electrons faster, decreasing resistivity<sup>28</sup>. Poor electrode contact can also alter resistivity values. To minimize poor electrode contact, it is recommended using flexible electrodes, electrically conductive jelly, or saturated sponges with wetting samples prior to measuring<sup>28</sup>. Concrete's resistivity depends on the microstructure and transport properties but is not a great indicator of durability performance due to lack of consideration to changes in the pore solution resistivity that influence the concrete resistivity measurement<sup>10,45</sup>.

### **2.2.2 Rapid Chloride Permeability Test (RCPT)**

Low-permeability concrete can lead to a more durable concrete by limiting media migration. The Rapid Chloride Permeability Test (RCPT), adapted as the ASTM C1202 "Standard Test Method for Electrical Indication of Concrete's Ability to Resist Chloride Ion Penetration" and AASHTO T277, "Standard Method of Test for Rapid Determination of the Chloride Permeability of Concrete," is a NDT method used to determine chloride permeability<sup>28,46</sup>. Prior to the RCPT, ponding tests were used to measure chloride permeability which involves taking

concrete samples to various depths of chloride typically for 90 days or more<sup>47</sup>. With chloride ingress through concrete being a slow process, the RCPT accelerates chloride migration by applying an electrical current. Upon proper preparation, a sample is placed

ASTM C1202 Classification <sup>1</sup>	Charge Passed (Coulombs) <sup>1</sup>	Resistivity (kOhm·cm) <sup>2</sup>
High	>4,000	<5.2
Moderate	2,000–4,000	5.2–10.4
Low	1,000–2,000	10.4–20.7
Very low	100–1,000	20.7–207
Negligible	<100	>207

Figure 18. Performance limits from RCPT with equivalent resistivity values<sup>49</sup>

in the apparatus that has the left side (–) filled with a 3% NaCl solution and the right side (+) filled with 0.3N NaOH solution illustrated in Figure 19<sup>47,48</sup>. 60 volts is applied across the sample and

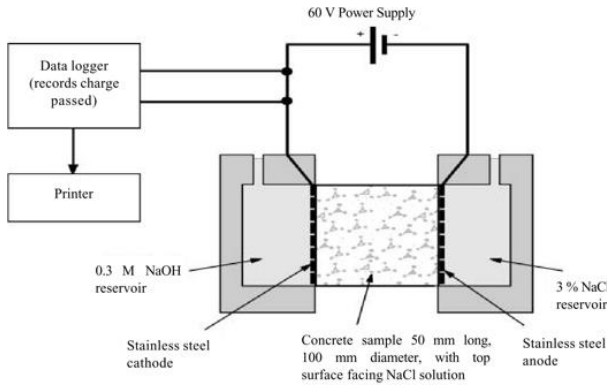


Figure 19. AASHTO T277 / ASTM C1202 RCPT setup<sup>48</sup>

current readings are taken every 30 minutes<sup>28,47</sup>. By integrating the current versus time, the total charge passed (Coulombs) is calculated. The Coulombs value is then referenced to the ASTM C1202 performance limits table to determine its classification as demonstrated in Figure 18<sup>49</sup>. Although titled to measure chloride permeability, RCPT truly measures resistivity as it applies a voltage divided by the current resulting in<sup>47,50</sup>:

$$Q_{RCPT} = \int_0^{6hr} I dt = \frac{V}{\rho \cdot \frac{L}{A}} \int_0^{6hr} dt = \frac{207000}{\rho} \quad \text{Equation 8.}$$

*RCPT – resistivity relationship<sup>49</sup>*

Where  $Q_{RCPT}$  is RCPT total charged passed (Coulombs);  $I$  is current (amps);  $v$  is voltage (60 volts);  $L$  is length (50 mm);  $A$  is sample area ( $100^2 \cdot \pi \text{ mm}^2$ );  $t$  is test time (6 hours); and  $\rho$  is sample resistivity ( $\Omega \cdot \text{m}$ ). Experimental data evaluating the RCPT – resistivity relationship have provided a reasonable match to concur the equation above<sup>49</sup>. With the RCPT being a resistivity measurement, factors that might have had little effect on chloride transport may have great effect on resistivity<sup>50</sup>. Considering RCPT is currently widely accepted in the concrete industry and highly criticized by researchers, it will continued to be used until other novel methods develop enough to measure

concrete permeability more precisely and reliably<sup>47,50</sup>. Formation factor testing in comparison to RCPT is more efficient in directly relating measured concrete properties to the long-term durability performance of concrete structures as seen in Figure 20<sup>9</sup>.

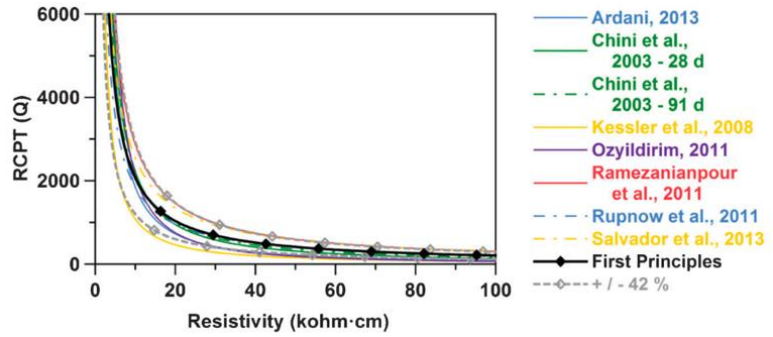


Figure 20. Correlation between RCPT and resistivity<sup>49</sup>

### 2.2.3 Formation Factor

Although standardized durability testing can be labor, cost, and time intensive, a common denominator is the transport of fluids/ions through the pore system<sup>51</sup>. The formation factor can determine true transport properties and directly relate to concrete durability<sup>52,53</sup>. Formation factor is no new concept, but rather a developing NDT method that can replace the existing RCPT<sup>9</sup>. Research has developed enough to establish a correlation between resistivity and chloride exposure test such as ASTM C1556, “Standard Test Method for Determining the Apparent Chloride Diffusion Coefficient of Cementitious Mixtures by Bulk Diffusion<sup>43,54</sup>”. Electrical measurements of porous materials can be described using the formation factor, the ratio of concrete resistivity and the pore solution resistivity; inversely equal to the product of porosity and tortuosity (*Equation 9*)<sup>28,55</sup>. As previously mentioned, a relationship between diffusivity and conductivity exists through the Nernst-Einstein equation and by applying Archie’s law to Equation 7, the correlation between bulk resistivity, pore solution resistivity, and porosity can be expressed as:

$$F = \frac{\rho}{\rho_o} = \frac{\sigma_o}{\sigma} = \frac{1}{\varphi \cdot \beta} = \frac{D_o}{D} \quad \text{Equation 9. Formation factor from Archie's law}^{28,55}$$

Where  $F$  is formation factor (unitless);  $\rho$  is bulk resistivity ( $\Omega \cdot m$ );  $\rho_o$  is pore solution resistivity ( $\Omega \cdot m$ );  $\beta$  is tortuosity (unitless); and  $\varphi$  is porosity of concrete (unitless)<sup>28,55</sup>. This correlation of the two resistivities provides a quantitative description of the pore system configuration<sup>51</sup>. Unlike

resistivity, formation factor provides an indication for pore configuration (total pore volume, tortuosity) and the pore solution in one equation<sup>55</sup>. A higher formation factor indicates slower ions movement, lower porosity and/or porosity tortuosity, and is more desirable for durability<sup>51</sup>. Building on the RCPT-resistivity relationship, formation factor can also be calculated from RCPT using the following conversion<sup>56</sup>:

$$Q_{RCPT} = V \cdot \frac{A}{L} \cdot t \cdot \frac{1}{\rho_o} \cdot \frac{1}{F} = \frac{206,830 \text{ Vms}}{\rho_o} \frac{1}{F} \quad \text{Equation 10. RCPT – formation factor conversion}^{56}$$

The charge passed in the RCPT is inversely related to the formation factor when assuming constant current and no sample heating<sup>56</sup>. The results of the RCPT demonstrate its dependency on both the fundamental microstructure parameter, formation factor, and the pore solution resistivity demonstrated in Figure 21<sup>56</sup>. Having such strong relation to already existing standard tests that are time, cost, and error intense create a great alternative that can be used to obtain other transport properties such as diffusion coefficients, and absorption<sup>55,56</sup>. Formation factor also inherits the factors affecting resistivity; to minimize changes to the DOS, DOH, and pore solution chemistry, the pore solution must be kept constant throughout<sup>52</sup>. The AASHTO TP 119 “Standard Method of Test for Electrical Resistivity of a Concrete Cylinder Tested in a Uniaxial Resistance Test” latest updates provide details for curing and conditioning and electrode setup specifically for formation factor<sup>43</sup>. Curing and conditionings option A, also known as the “bucket test,” provides a specific, simulated pore solution such that a constant pore solution conductivity of 0.127 S/m can be used in formation factor calculations<sup>43</sup>. This method avoids tedious measuring of pore solution conductivity and reliance on modeling<sup>57,58</sup>. With numerous durability mechanisms in existence, formation factor will not necessarily replace methods like RCPT; but it is more versatile in characterizing the transport and pore systems in terms of porosity, connectivity, and pore solution. Water absorption<sup>55</sup>.

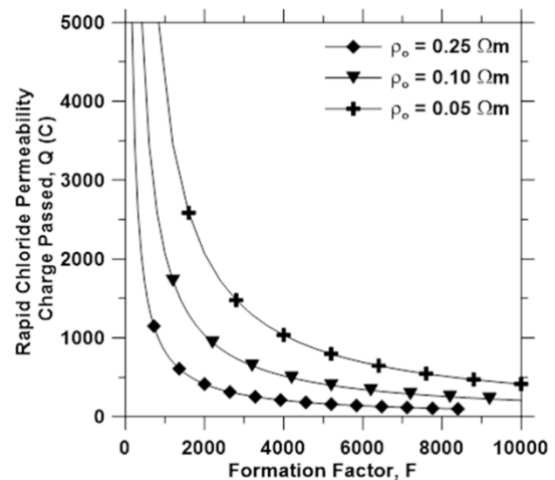


Figure 21. Correlation between RCPT and formation factor<sup>56</sup>

## 2.2.4 Mechanical Testing

Concrete mechanical testing has long been used due to easy execution and directly determining a hardened concrete quality even though samples are completely destroyed and not available for further testing<sup>7,15</sup>. Mechanical testing follows standards for evaluating one of the following strengths: compressive, flexural, or tensile strength<sup>8</sup>. Compressive testing is widely used as one of the oldest methods for determining strength. This is backed by the existing requirements for compressive strength in U.S. cement specifications detailed by cement type and categories for low (< 20 MPa), moderate (20-40 MPa), and high strength (>40 MPa)<sup>3,16</sup>. Testing commonly consists of measuring the maximum compressive load before failure for specimens cured under standard temperature-humidity conditions for a period of 28 days as illustrated in Figure 22<sup>16</sup>.



Figure 22. Schematic of splitting tensile test<sup>62</sup>

Flexural strength is mainly evaluated in pavement and reinforced steel design that measures modulus of rupture or measures the bonding force of paste or ability for a material to resist bending<sup>3,59</sup>. During testing, flexural strength is measured using the setup illustrated in Figure 23 and the flexural strength formula is used to calculate maximum stress when rupture occurs<sup>16,60</sup>. Tensile strength or ultimate tensile strength is important when considering structures such as dams that cannot rely on

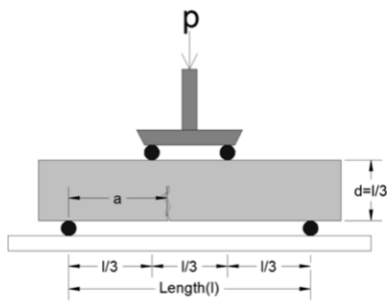


Figure 23. Concrete flexural strength setup<sup>60</sup>

compressive strength to determine its quality. This property provides stretch strength as the maximum tensile load failure divided by its cross-sectional area, which is commonly tested with a concrete cylinder under opposite compressive loads until splitting failure as illustrated in Figure 24<sup>61,62</sup>. Generally, tensile strength is lower than compressive strength with most correlations in literature being based on normal curing conditions and testing age of 28 days<sup>63</sup>.

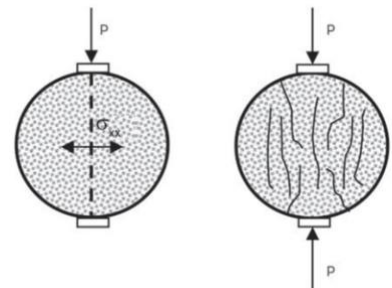


Figure 24. Concrete cylinder tested in compression<sup>3</sup>

## 2.2.5 Thermogravimetric Analysis

Thermogravimetric analysis (TGA) studies mass changes, be it a gain or a loss, as a function of time and/or temperature<sup>22</sup>. In the realm of cement and concrete, the focus becomes



Figure 26.  
Thermogravimetric  
analyzer furnace setup.

weight loss and seeing how chemical reactions such as combustion, dehydration, and decomposition leads to bonds breaking apart such as gypsum's water loss at higher temperatures<sup>22</sup>. Samples can be in the form of a liquid or a solid if the material being analyzed is known not to react dangerously (deadly off gas) with the sample pan material (platinum, alumina, or aluminum) and the set atmosphere (nitrogen compressed air, etc.). Sample mass typically are 10-20 milligrams for most applications and 50-100 milligrams for measuring volatiles or residues. Most TGA experiments are kinetic in nature and depend on temperature parameters such as limits, rate, and duration. Along with sample form and atmosphere set, these are the main parameters of focus for TGA setup. Once these parameters are set and a sample is weighed and loaded, the sample pan is placed into a furnace to

undergo the specified conditions. An example of the setup can be seen in Figure 26. Once the experiment run completed and data is collected via the software, a plot for a cellulose-gypsum composite analysis is demonstrated in Figure 25. The green curve is the main TGA curve that displays weight loss as temperature increase while the blue curve is the derivative to the TGA curve and demonstrates the rate of weight loss or gain as temperature increase. TGA can

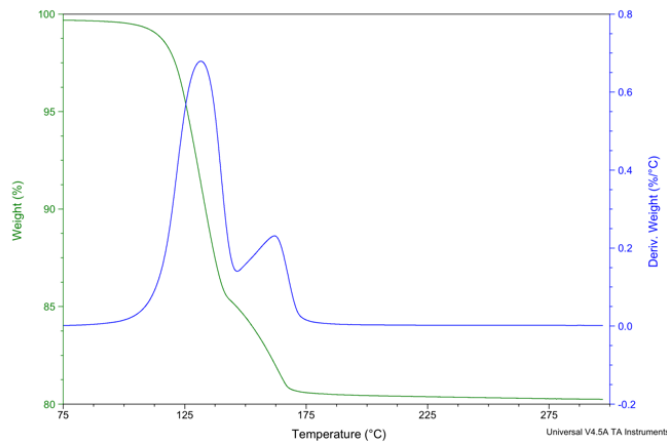


Figure 25. Cellulose-gypsum composite TGA curve (green) and DTG curve (blue)

help explain thermal stability, moisture content, and decomposition kinetics and much more.

### **2.3 Conclusion**

Testing for concrete's quality can be done in destructive and non-destructive ways. There currently is no catch-all method for determining or predicting concrete quality leading to the need for multiple methods being required to be applied for a full, confident analysis. With a need to be more efficient with data collection, non-destructive methods such as formation factor do a great job of development improvements on existing test methods such as rapid chloride permeability test (RCPT). Formation factor is a simple, faster, and inexpensive NDT method when applied correctly. Like many novel methodologies, formation factor application and reliability are still in development. Although formation factor's trade-off is the significant sensitivity to geometry, temperature, and curing and storage conditions, it shows promise in becoming essential as it is being implemented within concrete industry standardization such as the AASHTO TP 119 for durability assessment of cement and concrete.

### **3. ASSESSING THE EFFECT OF CELLULOSE NANOCRYSTALS ON CEMENT'S RESISTANCE TO CHLORIDE INGRESS USING THE FORMATION FACTOR**

#### **3.1 Introduction**

Considering the research advancements previously mentioned, there is still a need for further knowledge development of the interactions occurring between CNCs and cement particles upon hydration and into curing. While previous research has focused on a limited range of cement or CNC source material, this chapter looks at various cements and CNC source materials at early and late ages to better understand the CNC-cement interactions. This chapter focuses on assessing the effect of CNC on cement's resistance to chloride ingress using the formation factor methodology. The materials were characterized prior to mixing and final samples were analyzed using formation factor methodology.

#### **3.2 Materials**

The ordinary portland cement (OPC) used was a standard Type I/II, two variants of Type III, and a Type V as per ASTM C150, Standard Specification for Portland Cement<sup>64</sup>. The chemical composition of all cements used is shown in Table 1. While Type I/II is the most widely used OPC, Type III and Type V cements were used due to their finer particle size and low aluminate content respectively. The OPC Type IIIA was a cement Type III provided by Purdue University's Charles Pankow laboratory (Buzzi Unicem, Greencastle, IN). The OPC Type I/II, OPC Type IIIB, and OPC Type V were provided by Oregon State University's (OSU) civil engineering department via compositional analysis (Ash Grove, Durkee, OR).

Table 1. Cement composition analysis by mass percentage.

Oxide	Mass (%)			
	Type I/II	Type IIIA	Type IIIB	Type V
Silicon dioxide (SiO <sub>2</sub> )	20.1	19.50	21.5	20.62
Aluminum oxide (Al <sub>2</sub> O <sub>3</sub> )	4.7	5.14	3.5	2.62
Ferric oxide (Fe <sub>2</sub> O <sub>3</sub> )	3.5	2.76	3.1	4.44
Calcium oxide (CaO)	63.7	62.86	63.3	63.98
Magnesium oxide (MgO)	0.7	3.04	3.5	2.26
Sulfur trioxide (SO <sub>3</sub> )	3.1	4.01	3.0	2.86
Loss on Ignition	2.6	1.24	0.9	0.72
Limestone	4.0	-	-	-
Insoluble residue	0.3	0.25	0.21	-
Total Alkalies as Na <sub>2</sub> O	0.51	0.69	0.22	0.08
C <sub>3</sub> S*	53	57.8	58	71.54
C <sub>2</sub> S*	18	12.3	10.93	-
C <sub>3</sub> A*	7	9	4	0
C <sub>4</sub> AF*	11	8.4	9	-
Blaine fineness (m <sup>2</sup> /kg)	364	587	556.5	305

\* Cement chemistry notation: C = CaO, S = SiO<sub>2</sub>, A = Al<sub>2</sub>O<sub>3</sub>, F = Fe<sub>2</sub>O<sub>3</sub>.

A total of four cellulose nanocrystal source materials were used and are listed with their characteristics on Table 2. All CNCs were in the form of an aqueous suspensions with varying solid contents and sourced from wood pulp. They were purchased from partnering industry partners Blue Goose Biorefineries (Saskatoon, SK, Canada) and Forest Products Laboratory (Madison, WI)<sup>65</sup>.

Table 2. Characteristics of cellulose nanocrystals used.

CNC Type	Treatment	Surface Functionality (mmol/g)		Aqueous suspension (%)
		Carboxylate content	Sulfate content	
BGB Ultra <sup>2</sup>	Transition metal catalyzed oxidation	0.15	-	8
FPL 117	Sulfuric acid hydrolysis	-	0.3	10.4
FPL 120	Sulfuric acid hydrolysis and TEMPO oxidation	0.7	0.3	10.8
FPL 115F	Sulfuric acid hydrolysis	-	0.3	10.6

BGB Ultra<sup>2</sup> CNC was produced from a viscose-grade dissolving pulp that has an isolation method that is oxidative in nature via a transition metal catalyzed oxidation process resulting in an aqueous suspension with carboxylate surface functionality of approximately 0.15 mmol/g therefore not involving acid hydrolysis. FPL 115F, 117, and 120 CNC are also sourced from wood pulp but differ in processing. CNC FPL 115F and 117 underwent sulfuric acid (Columbus Chemical Industries, Columbus, WI) (64% by weight) hydrolysis to dry cellulose for 60 minutes at 45 °C in an oxygen-free atmosphere in order to hydrolyze the amorphous cellulose to sugars and functionalize the crystalline surface<sup>5</sup>. After hydrolysis, CNCs are diluted to stop chemical processes and remove color using reverse osmosis water and sodium chlorite<sup>5</sup>. Lastly, the acid is neutralized via use of sodium hydroxide then cleaned and concentrated via purification resulting in an aqueous suspension with sulfate surface functionality of approximately 0.3 mmol/g<sup>5</sup>. FPL 120 CNC is further processed by applying TEMPO ((2,2,6,6-Tetramethylpiperidin-1-yl)oxyl) and hypochlorite oxidation chemistry in addition to the previously mentioned treatment, resulting in additional carboxylate surface functionality of approximately 0.7 mmol/g to the existing sulfate surface functionality of approximately 0.3 mmol/g.

### 3.2.1 Sample Preparation

Sample preparation and storage started with mix design which was established in conjunction with OSU. Each profile consisted of a specified cement type, water-to-cement (w/c) ratio, CNC concentration (CNC/cement volume percent), and CNC source material. In addition, each set of profiles included a sample with no CNC in the mixture as a reference baseline. This

results in each profile having nine mix designs (one non-CNC, and eight CNC; four of each of the two concentrations) and a total of 36 mix designs. These mix profiles are outlined in the test matrix is shown in Table 3.

*Table 3. Mix design test matrix*

Profile Name	Cement type	w/c ratio	CNC source material	CNC/cement vol %
FF1 FF2	Type I/II	0.3	BGB Ultra <sup>2</sup>	0.2, 0.5
			FPL 115F	0.2, 0.5
		0.35	FPL 117	0.2, 0.5
			FPL 120	0.2, 0.5
FF3	Type III: A	0.35	BGB Ultra <sup>2</sup>	0.2, 0.5
			FPL 115F	0.2, 0.5
			FPL 117	0.2, 0.5
			FPL 120	0.2, 0.5
FF4	Type III: B	0.35	BGB Ultra <sup>2</sup>	0.2, 0.5
			FPL 115F	0.2, 0.5
			FPL 117	0.2, 0.5
			FPL 120	0.2, 0.5
FF5 FF6	Type V	0.3	BGB Ultra <sup>2</sup>	0.2, 0.5
			FPL 115F	0.2, 0.5
		0.35	FPL 117	0.2, 0.5
			FPL 120	0.2, 0.5

The cement paste mixtures consisted of deionized (DI) water, cement powder, and CNC slurries. It started with CNC being measured and placed into a 50 mL centrifuge tube with deionized (DI) water. This was then vortexed mixed for 60 seconds (Mortexer Vortex Mixer; 115V, 200-3400 rpm) at approximately 70% / 2200 rpm. The resulting suspension was poured in a beaker and the remaining DI water required for the mix was added; this was then spatula-stirred for 60 seconds. The cement powder was then measured into a mixing bowl. Immediately after adding the suspension to the cement in the mixing bowl, it was vacuum mixed at 400 rpm and 100% vacuum for 90 seconds (Renfert Twister Evolution Mixer; 110V). After this initial mixing, the cement

paste was spatula-stirred for 30 seconds to prevent buildup along the bowl wall. It was then run through another 90 second mix cycle. The final cement paste was set into a 2” x 4” plastic cylinder mold. To eliminate unwanted air pores, the cylinder was vibrated at 50% for 60 seconds (Whip Mix General Purpose Vibrator; 115V, 50Hz). The cylinder was then capped with plastic caps that contained 3 layers of saver liner paper for a smoother sample top surface upon demolding. The capped cylinder was then set in a desiccator of high humidity (85-95% relative humidity) to cure for three days. Three days was chosen as the curing time due to Cement Type V’s shrinkage and higher excess water curing better after three days rather than one. After curing, the sample was demolded, height was recorded (for resistivity geometry correction factor) and immediately stored in a 5 gallon bucket containing a simulated pore solution for a minimum of six days. This was in accordance with AASHTO TP 119 which is followed for formation factor calculations<sup>43</sup>. The pore solution conditioning prepared was Option A of AASHTO TP 119, “Immersion of specimens in a calcium hydroxide saturated simulated pore solution.”<sup>43</sup> The solution consists of 7.6g/L NaOH (0.19M); 10.64g/L KOH (0.19M); 2g/L Ca(OH)<sub>2</sub> and made in a 5 gallon bucket using 13250 g water, 102.6g NaOH, 143.90g KOH and 27g Ca(OH)<sub>2</sub> for a final solution of 18.9 L<sup>43</sup>. Establishing this pore solution allows for using an estimated pore solution resistivity of 0.127 Ω-meters. All samples were prepared and stored at standard temperatures for testing, i.e., 23 ± 2°C<sup>43</sup>.

### 3.3 Methods

#### 3.3.1 Uniaxial Resistance and Formation Factor

Samples were only removed when taking measurements from days 9 to 28. This time range is due to three days of curing followed by the six minimum days in solution (start at day 9) and ending with the industry standard of 28 days of which 99% of strength is developed<sup>66</sup>. Although most strength development has occurred, hydration is still ongoing and gradually continues over time as does resistance. The AASHTO TP 119 uniaxial resistance measurement configuration

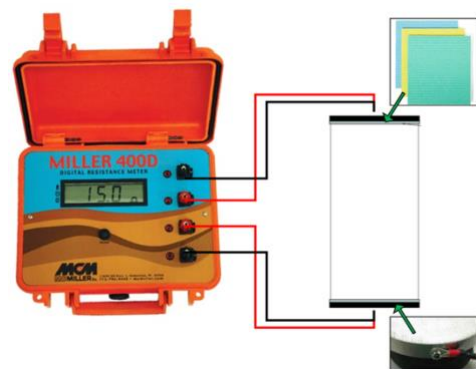


Figure 27. Uniaxial resistance equipment configuration<sup>67</sup>

consisted of a cylinder sample, two sponges, and a resistivity apparatus. The resistivity apparatus

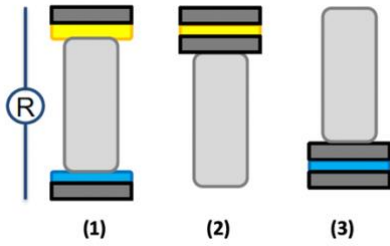


Figure 28. Resistance measurements setup: (1) sample and sponges (2) top sponge (3) bottom sponge

used was a Miller 400D digital resistance meter (Sebastian, FL) with stainless steel electrode plates connected via screw eyelet connectors as shown in Figure 27<sup>67</sup>. The sponges used were cellulose sponge cloth (Full Circle, New York, NY)<sup>68</sup>. Upon cutting out the sponges in the shape of the electrode they are immersed in the same simulated pore solution used to store samples. For each recording three measurements were taken: (1) sample with sponges (2) top sponge (3) bottom sponge as

shown in Figure 28. To start, sponges were removed and placed on electrodes. Then one sample at a time is removed from storage solution, excess liquid is blotted off, and finally placed on the bottom electrode and sponge with the top electrode and sponge placed immediately on top. After 30 seconds, a resistance measurement is recorded. This is repeated for each sample with a re-soaking of both sponges for each new measurement. The final sample resistance is then calculated using the equation below:

$$R_{cylinder} = R_{cmeasured} - R_{top\ sponge} - R_{bottom\ sponge} \quad \text{Equation 11. Final resistance calculation}^{43}$$

Where  $R_{cylinder}$  is the resistance of the sample ( $\Omega$ );  $R_{measured}$  is the measured resistance including the conductivity media (sponges) ( $\Omega$ );  $R_{top\ sponge}$  is the measured resistance of the top conductive medium (top sponge) ( $\Omega$ ); and  $R_{bottom\ sponge}$  is the measured resistance of the bottom conductive medium (bottom sponge) ( $\Omega$ )<sup>43</sup>. The final resistance was then converted to resistivity by applying a geometry correction factor for a cylinder:

$$\rho = R_{cylinder} \cdot \frac{A}{L} = R_{cylinder} \cdot \frac{2 \cdot \pi \cdot r^2}{height} \quad \text{Equation 12. Resistivity equation for uniaxial cylinder}^{43}$$

Where  $\rho$  is the electrical resistivity of the sample ( $\Omega\cdot m$ );  $R_{cylinder}$  is the resistance of the sample;

$A$  is the cross sectional area of the sample ( $m^2$ ); and  $L$  is the length of sample (m).

The sample resistivity and pore solution resistivity were then plugged into Equation 9 to calculate a formation factor value. An outline of sample

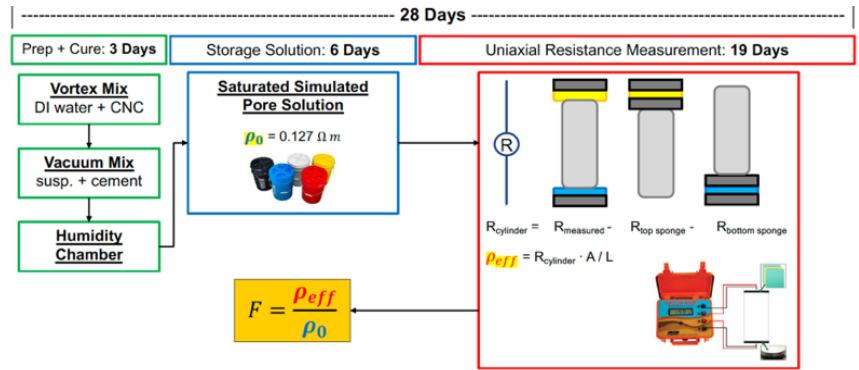


Figure 29. Sample preparation summary

preparation and process is illustrated in Figure 29. All data points had a standard error as the error bar that never exceeded 4%. The equation for standard error is below:

$$SE = \frac{\sigma}{\sqrt{n}}$$

Equation 13.  
Standard error formula

Where  $\sigma$  is the sample standard deviation and  $n$  is the number of samples. RStudio software was used for plotting of all data.

### 3.3.2 Chloride Ingress

To put formation factor data in context, a chloride diffusion approach transforms formation factor into chloride ingress, a common concrete engineering property<sup>69</sup>. Inputting formation factor into the Error Function Solution to Fick's Second Law and Nernst-Einstein equation is as follows:

$$\frac{C_{x,t} - C_0}{C_s - C_0} = 1 - erf\left(\frac{x}{2\sqrt{\frac{D_0}{F} \cdot t}}\right)$$

Equation 14.  
Fick's Second Law with formation factor<sup>69</sup>

Where  $C_{x,t}$  is the chloride concentration at time  $t$  (seconds) at depth  $x$  (meters) (% by mass of concrete);  $C_0$  is the background chloride concentration (% by mass of concrete);  $C_s$  is the chloride

concentration at the surface (% by mass of concrete);  $D_0$  is the chloride ion self-diffusion coefficient ( $\text{m}^2/\text{s}$ )<sup>69</sup>. In order to calculate the life-cycle estimation of the samples against chloride ingress, the following values were selected: 50mm for  $x$ ; 0.05% for  $C_{x,t}$  corresponding to corrosion's chloride concentration threshold; 0.02% for  $C_0$ ; 0.5% for  $C_s$  for moderate chloride exposure; and  $19 \times 10^{-10} \text{ m}^2/\text{s}$  for  $D_0$ . More of the approach and selection of values can be found in literature<sup>53,69</sup>.

## 3.4 Results and Discussion

### 3.4.1 Formation Factor

Figure 30 to Figure 35 and Figure 36 to Figure 41 demonstrate formation factor against time for 0.2% and 0.5% CNC concentration respectively. The plots include a general smoothing curve to see the trend over time. The initial hypothesis was that the addition of CNC to cement will improve formation factor across all cement types. Profile FF1 (Figure 30), CNC addition demonstrated a slight increase over time across all CNCs added. Profile FF2 (Figure 31) demonstrated no significant change over time which can be explained by the higher water content causing greater dispersion resulting in less C-S-H crystal bridging compared to FF1<sup>70</sup>. Profile FF3 (Figure 32) demonstrated a slight decrease in comparison to profile FF4 (Figure 33) demonstrated a slight increase. Considering they are both Type III OPC from different sources, they demonstrated opposing trends within different ranges. Profile FF5 (Figure 34) and profile FF6 (Figure 35) demonstrated an increase in formation factor across all CNC additions. Profile FF6 has a lower formation factor value range due to the increase in water previously mentioned. It is important to note that naturally electrical resistivity will increase with age due to continued hydration and the resulting product taking up more and more space within microstructure pores<sup>10</sup>. Another note is that BGB Ultra<sup>2</sup> CNC usage in OPC Type V at higher concentrations demonstrated the greatest improvement in formation factor.

Figure 42 to Figure 47 and Figure 48 to Figure 53 illustrate formation factor values against CNC concentration for early (28 days) and late ages (minimum 300 days) respectively. For comparison, the non-CNC formation factor value was compared to the average of all CNC formation factor values for each CNC concentration. For profiles FF5 and FF6 at early age at 0.2% CNC concentration, there is a significant increase of 15.534% and 31.099% respectively. For early

age at 0.5% CNC concentration, Aa similar increase of 19.721% and 33.462% respectively is demonstrated. At late age for profile FF5, there is a reduced increase for the 0.2% CNC and 0.5% CNC of 11.207 and 11.881 percent respectively. Lastly, FF1 at late age demonstrated an increase of 8.466% and 11.428% for CNC concentrations 0.2% and 0.5% respectively.

### 3.4.2 Chloride Ingress

Formation factor, a microstructure material property, through the Nernst-Einstein relationship relates to resistivity and chloride diffusion coefficient<sup>53</sup>. In combination with the error function solution to Fick’s second law, an estimation for chloride ingress was calculated using formation factor values<sup>53</sup>. Chloride ingress in years is provided in the table below:

*Table 4. CNC cement estimated time to corrosion initiation for moderate chloride exposure (early and late ages)*

Profile No	Early age (28 days)					Late age (300+ days)				
	No CNC	0.2% CNC	Δ%	0.5% CNC	Δ%	No CNC	0.2% CNC	Δ%	0.5% CNC	Δ%
<b>FF1</b>	0.686	0.689	0.360	0.682	-0.642	0.794	0.861	8.466	0.885	11.428
<b>FF2</b>	0.868	0.901	3.883	0.900	3.755	1.344	1.320	-1.836	1.357	0.961
<b>FF3</b>	0.962	0.943	-2.032	0.951	-1.157	1.261	1.300	3.114	1.250	-0.885
<b>FF4</b>	0.729	0.816	11.949	0.815	11.863	1.067	1.017	-4.711	1.045	-2.039
<b>FF5</b>	0.744	0.882	18.515	0.919	23.506	0.887	0.987	11.207	0.993	11.882
<b>FF6</b>	0.384	0.583	52.039	0.598	55.991	0.642	0.658	2.499	0.675	5.176

For early age, profiles FF4, FF5, FF6, show significant increase in estimated time to corrosion initiate under moderate chloride exposure. For late age, profiles FF1 and FF5 show significant increase. While this approach establishes a relationship between formation factor and chloride ingress, it is considered conservative due to not taking into account aging effects of transport properties and is better labeled a life-cycle estimation using a diffusion-based model<sup>53,69</sup>.

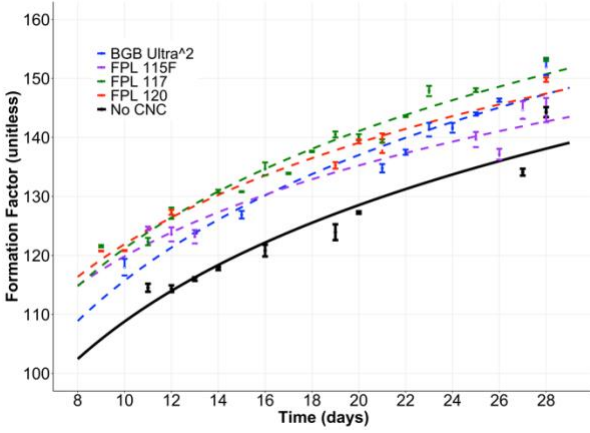


Figure 30. FF1 vs time (Type I/II, 0.3 w/c, 0.2% CNC)

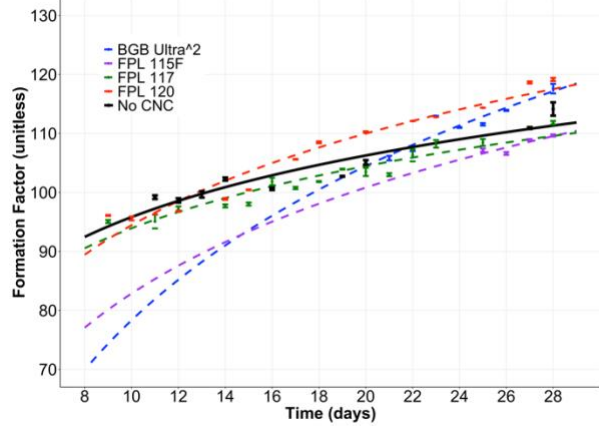


Figure 31. FF2 vs time (Type I/II, 0.35 w/c, 0.2% CNC)

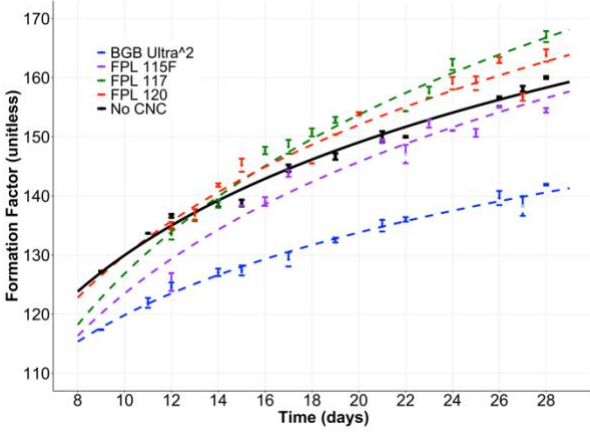


Figure 32. FF3 vs time (Type IIIA, 0.35 w/c, 0.2% CNC)

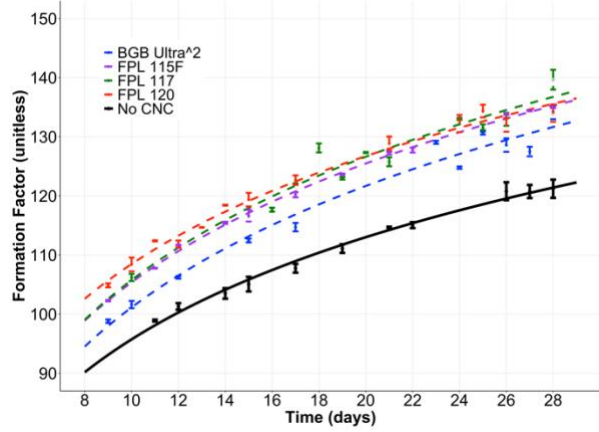


Figure 33. FF4 vs time (Type IIIB, 0.35 w/c, 0.2% CNC)

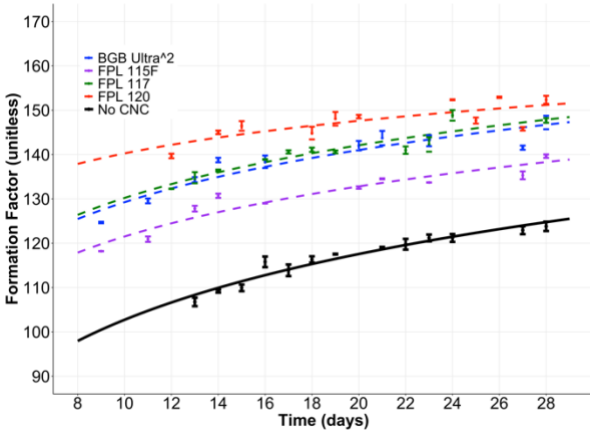


Figure 34. FF5 vs time (Type V, 0.3 w/c, 0.2% CNC)

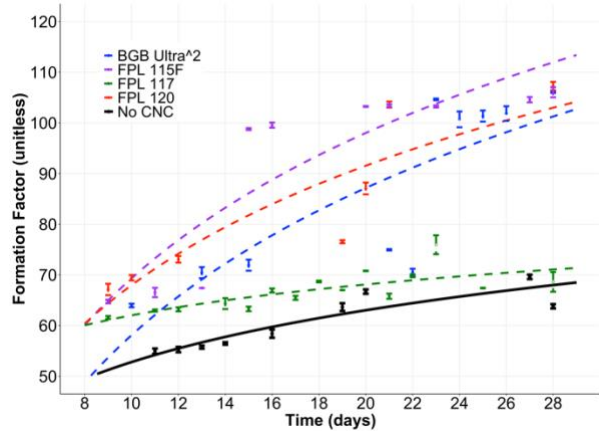


Figure 35. FF6 vs time (Type V, 0.35 w/c, 0.2% CNC)

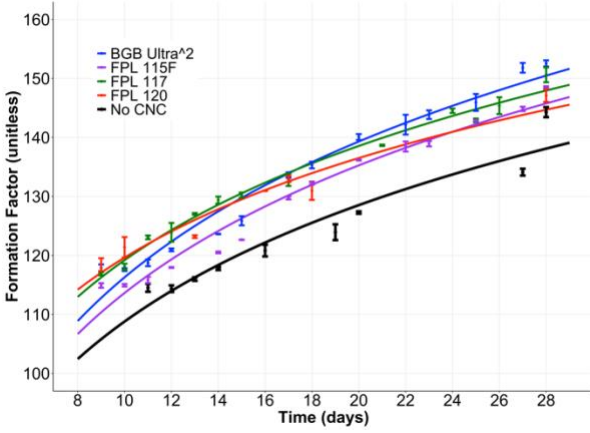


Figure 36. FF1 vs time (Type I/II, 0.3 w/c, 0.5% CNC)

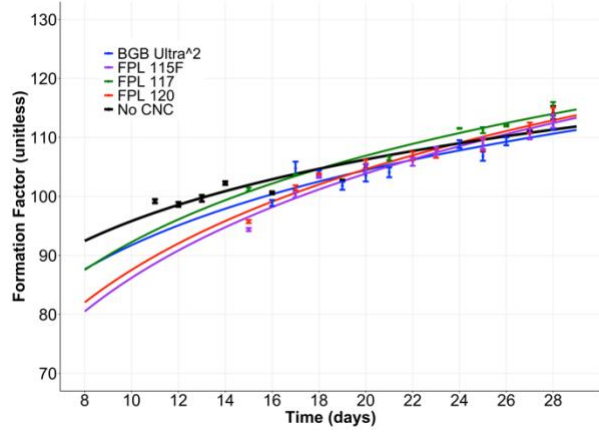


Figure 37. FF2 vs time (Type I/II, 0.35 w/c, 0.5% CNC)

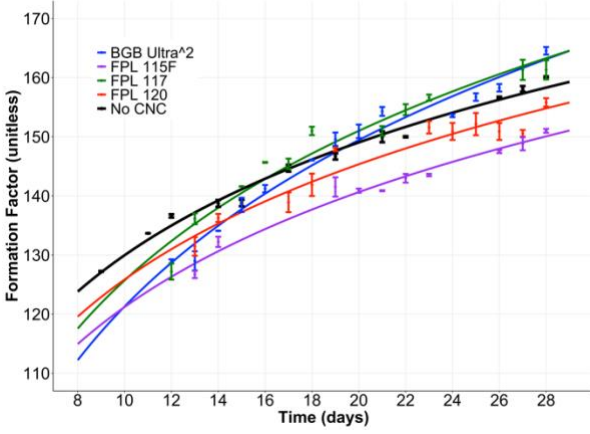


Figure 38. FF3 vs time (Type IIIA, 0.35 w/c, 0.5% CNC)

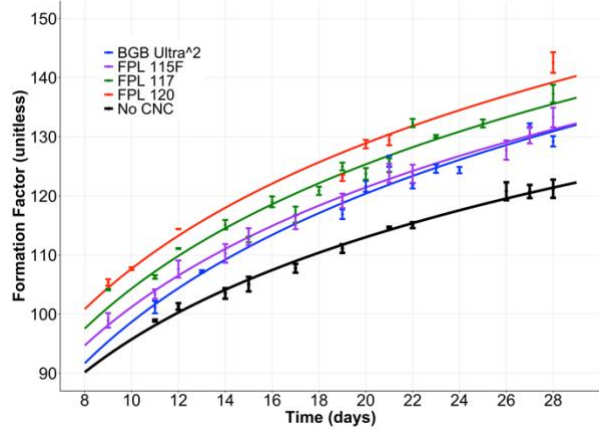


Figure 39. FF4 vs time (Type IIIB, 0.35 w/c, 0.5% CNC)

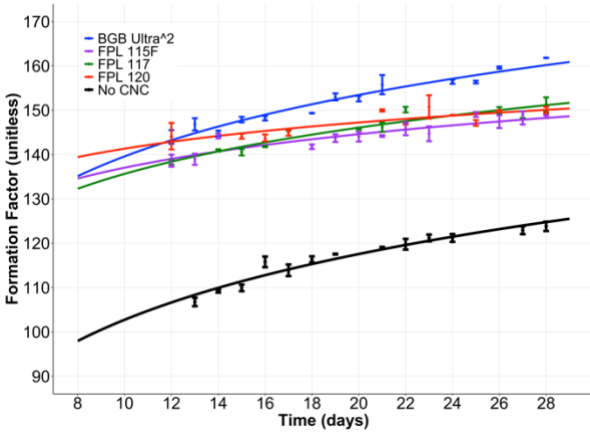


Figure 40. FF5 vs time (Type V, 0.3 w/c, 0.5% CNC)

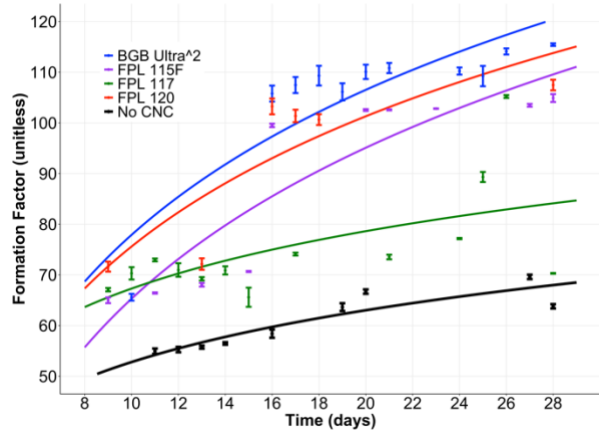


Figure 41. FF6 vs time (Type V, 0.35 w/c, 0.5% CNC)

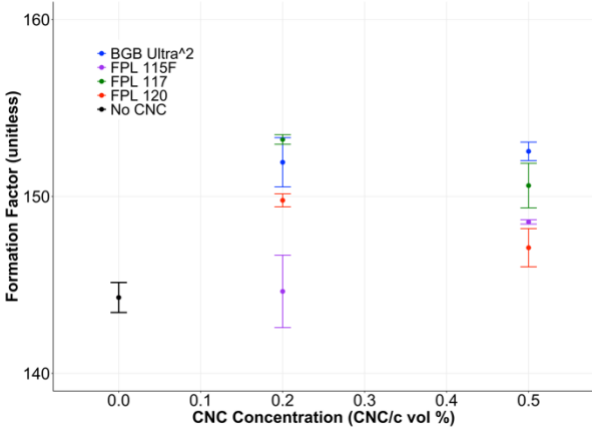


Figure 42. FF1 vs CNC concentration (Type I/II, 0.3 w/c, early age)

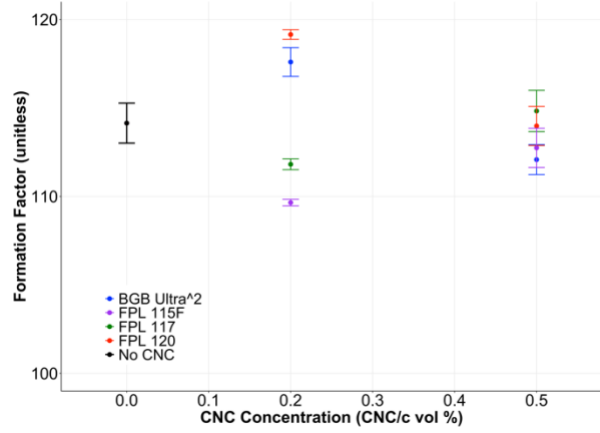


Figure 43. FF2 vs CNC concentration (Type I/II, 0.35 w/c, early age)

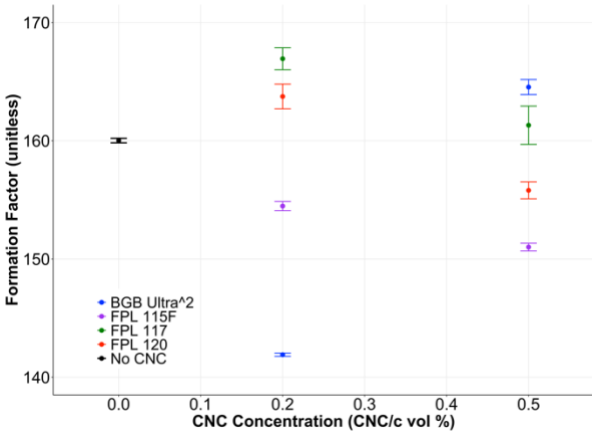


Figure 44. FF3 vs CNC concentration (Type IIIA, 0.35 w/c, early age)

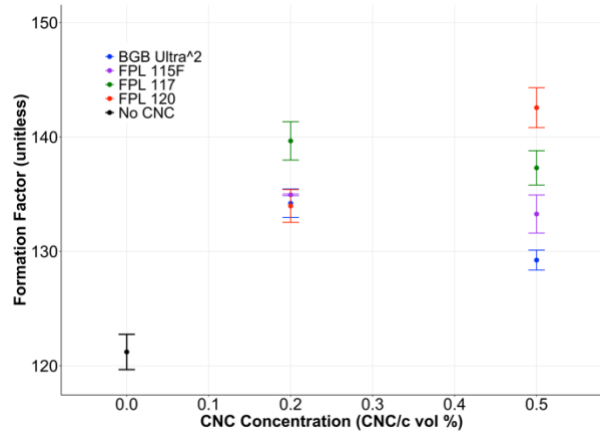


Figure 45. FF4 vs CNC concentration (Type IIIB, 0.35 w/c, early age)

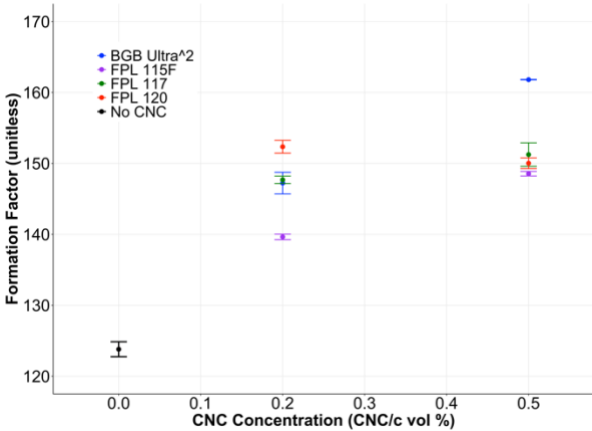


Figure 46. FF5 vs CNC concentration (Type V, 0.3 w/c, early age)

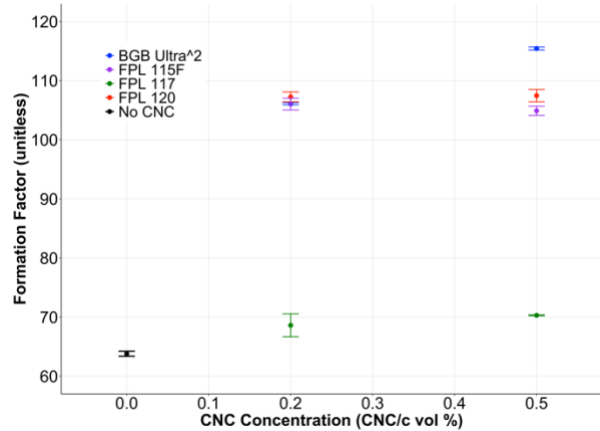


Figure 47. FF6 vs CNC concentration (Type V, 0.35 w/c, early age)

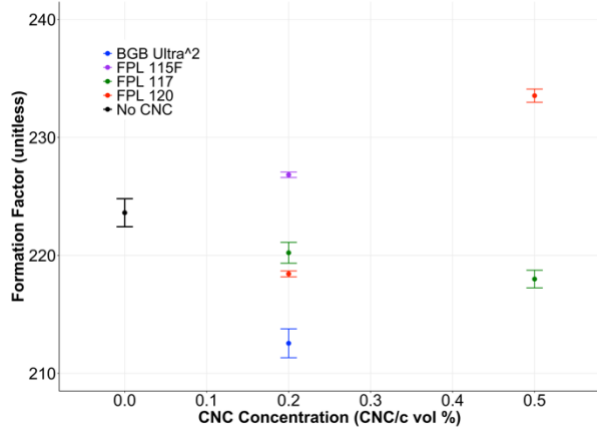


Figure 48. FF1 vs CNC concentration (Type I/II, 0.35 w/c, late age)

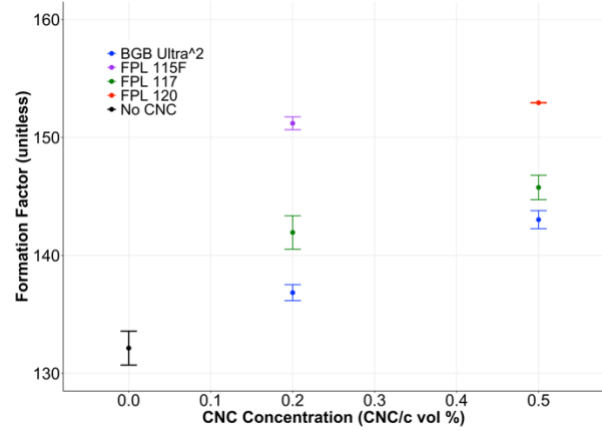


Figure 49. FF2 vs CNC concentration (Type I/II, 0.3 w/c, late age)

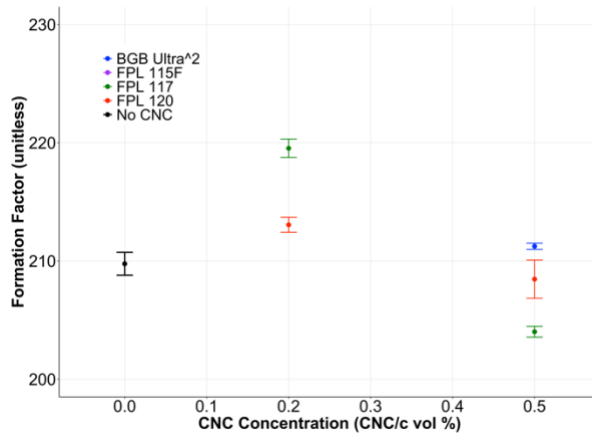


Figure 50. FF3 vs CNC concentration (Type IIIA, 0.35 w/c, late age)

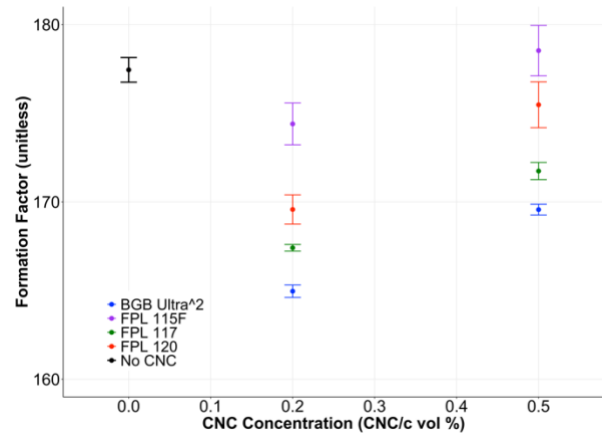


Figure 51. FF4 vs CNC concentration (Type IIIB, 0.35 w/c, late age)

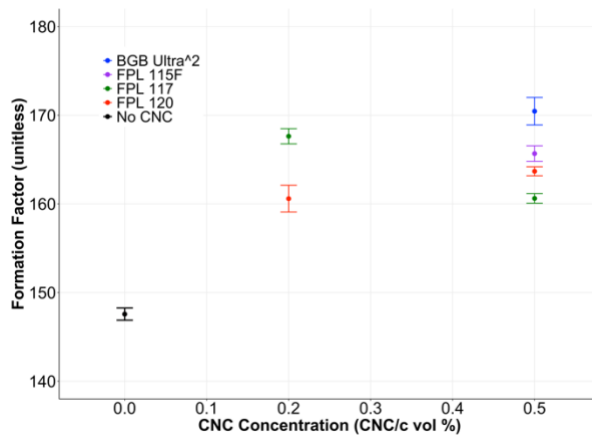


Figure 52. FF5 vs CNC concentration (Type V, 0.3 w/c, late age)

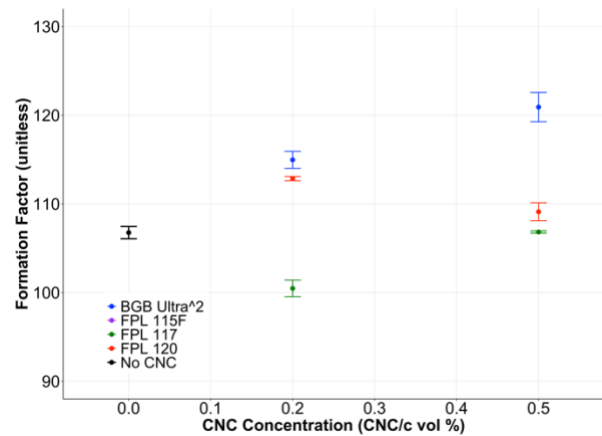


Figure 53. FF6 vs CNC concentration (Type V, 0.35 w/c, late age)

### 3.5 Conclusions

Four CNCs and four cements were used in this chapter to investigate the effect on the resistance to chloride ingress for cement with CNC as an additive through formation factor methodology. The conclusion is as followed:

- Formation factor values gradually increasing over time was confirmed due to ongoing hydration occurring that increase a sample's resistance
- Addition of CNC to cement at small concentrations does not always improve formation factor and may be dependent on cement type, CNC source materials, and/or CNC processing method but needs further investigated
- Of the CNCs and OPCs used, a significant increase in formation factor over time was demonstrated when CNC was combined with Type V OPC (Profile FF5 and FF6) for both CNC concentrations used
- BGB Ultra<sup>2</sup> CNC demonstrated the highest increase in formation factor in Type V OPC (Profile FF5 and FF6) for the higher concentration (0.5% CNC)
- Higher water-to-cement ratios reduced formation factor value ranges and can be attributed to the increase in water resulting in greater dispersion and lower formation factor values
- OPC Type IIIB and Type V (Profiles FF4, FF5, FF6) demonstrated a significant increase in formation factor at early ages when CNC was added
- OPC Type V with a water-to-cement ratio of 0.3 (Profile FF5) demonstrated a significant increase in formation factor for both early and late ages when CNC was added
- OPC Type I/II with a water-to-cement ratio of 0.3 (Profile FF1) demonstrated a significant increase in formation factor for late age when CNC was added
- Using the Nernst-Einstein relationship and Fick's second law, an estimation for chloride ingress was calculated and demonstrated significant increase for profiles FF4, FF5, and FF6 at early ages and increase for profiles FF1 and FF5 at late ages

## 4. THE INFLUENCE OF CELLULOSE NANOCRYSTALS AND NANOFIBRILS ON GYPSUM MECHANICAL PROPERTIES AND THERMAL ANALYSIS

### 4.1 Introduction

As previously mentioned, it is important to continue to develop the knowledge of interactions that are occurring between cellulose nanomaterials (CNMs) and cement. To take a closer look at what may be happening, the interaction between CNMs and gypsum should be investigated as gypsum is one of the components of cement. In cement, gypsum is a material that delays hydration and can be found in many residential and commercial buildings that help fight the spread of fire. This can help lead to new developments of CNM binder applications being commercialized. Correia et al. reported increase in mechanical properties when introducing nanofibril cellulose to gypsum plates<sup>36</sup>. This chapter's focus is to investigate the influence cellulose nanomaterials have on mechanical properties and thermal analysis when added to plaster of Paris and water as it forms into gypsum. Specifically, the influence from two CNMs, cellulose nanocrystals and cellulose nanofibrils, on mechanical properties will be investigated. The initial hypothesis was that the addition of these CNMs to gypsum will increase mechanical properties through improved interlinking within the gypsum network and reflect the stoichiometry mass loss in its thermal analysis<sup>71</sup>.

### 4.2 Materials

Commercially available United States Gypsum Company No. 1 pottery plaster (USG No. 1) plaster of Paris powder was used in this study and its typical physical properties are provided in Table 5 (Chicago, IL)<sup>72</sup>.

*Table 5. USG No.1 pottery plaster typical physical properties*

Normal Consistency (water/product lbs)	Compressive Strength (psi; MPa)	Density (lbs/ft <sup>2</sup> ; kg/m <sup>2</sup> )	Maximum Expansion (%)
70/100	<u>1hr after set</u> : 1000; 6.9	<u>Wet</u> : 99; 1586	0.21
	<u>Dry</u> : 2400; 16.5	<u>Dry</u> : 69; 1105	

Two cellulose nanomaterials were used in this experiment and are listed with their corresponding characteristics on Table 6 (University of Maine, Orono, ME)<sup>73</sup>. The cellulose nanocrystals (CNCs) and cellulose nanofibrils (CNFs) were in the form of an aqueous suspension with varying solids contents. The mechanically fibrillated CNF is a CNF-water slurry of 3 wt% and the CNC is sulfuric acid-derived CNC-water slurry of 11.9 wt%<sup>73,74</sup>. The method for CNC processing was discussed in more detail in the previous chapter.

*Table 6. Characteristics of cellulose nanomaterials (CNMs) used*

<b>Cellulose type</b>	<b>Source</b>	<b>Treatment</b>	<b>Average particle length (nm)</b>
CNC	viscose-grade dissolving pulp	transition metal catalyzed oxidation	150-200
CNF	wood pulp	mechanical separation	several hundred microns

The cellulose-gypsum composite mix design profiles used are shown in Table 7 with varying water-to-binder (w/b) ratio, CN source material, and weight percent. Considering the common w/b ratio is 1:2, a higher and lower ratio were also tested. Keeping the amount of plaster of Paris the same, the water amount was adjusted in order to achieve the corresponding ratio.

*Table 7. Cellulose-gypsum composite mix design profiles*

<b>Cellulose type</b>	<b>w/b ratio</b>	<b>CN/gypsum vol %</b>	<b>Profile No.</b>
REF	1:1.5	0	1
	1:2	0	9
	1:2.5	0	15
CNC	1:1.5	0.1, 0.33, 1, 3.33	2, 3, 4, 5
	1:2	0.1, 0.33, 1	10, 11, 12
	1:2.5	0.033, 0.1, 0.33	16, 17, 18
CNF	1:1.5	0.1, 0.33, 1	6, 7, 8
	1:2	0.1, 0.33	13, 14
	1:2.5	0.033, 0.1	19, 20

#### **4.2.1 Sample Preparation**

40 grams of plaster of Paris, the appropriate amount of CNC or CNF undiluted slurry, and water were weighed into a plastic jar and mixed in a FlakTek SpeedMixer planetary centrifugal mixer at 2000 rpm for 1 minute (Landrum, SC). The mixed slurry was then cast into 0.5 inch diameter, 2 inches tall cylinders by pouring into silicone molds, demolded after 24 hours, and stored in Ziploc plastic bags (Bay City, MI). After two weeks, the cylinders were oven dried at 50 °C until the weight stabilized after approximately 72 hours.

### **4.3 Methods**

#### **4.3.1 Compressive Strength**

To examine compressive properties, samples were tested in uniaxial compression using an MTS machine with stainless steel platelets (MTS Systems, Eden Prairie, MN). A loading rate of 0.1 mm/min was used for all samples and the peak load was used in strength calculations. A total of 5 samples were tested for each composite profile and averaged. All averaged data points had a standard error as the error bar. The equation for standard error is below:

$$SE = \frac{\sigma}{\sqrt{n}}$$

Equation 15.  
Standard error formula

Where  $\sigma$  is the sample standard deviation and  $n$  is the number of samples.

### 4.3.2 Thermogravimetric Analysis (TGA)

After compressive strength testing, the remains were finely grounded into a powder for TGA using a mortar and pestle. Approximately 2 milligrams of each sample powder were placed in an aluminum crucible that was semi-hermetically sealed with a lid with a hole. This crucible setup was necessary in order to achieve separation of the two overlapping gypsum dehydration reactions that occur during heating<sup>26</sup>. Otherwise a single step curve from dihydrate to anhydrite is observed due to no water vapor pressure being created from the crucible to prevent early onset evaporation as shown in Figure 54<sup>24,25</sup>. This crucible was then placed onto a Platinum 100  $\mu$ L TGA pan and analyzed from 75 °C to 300 °C with a heating rate of 5 °C per minute in an air atmosphere at a flow rate of 60 ml/min. The TGA equipment used was a TA Instruments Q50 thermogravimetric analyzer along with the TA Instruments Universal Analysis software to obtain TGA curves and Derivative thermogravimetry (DTG) curves (New Castle, DE).

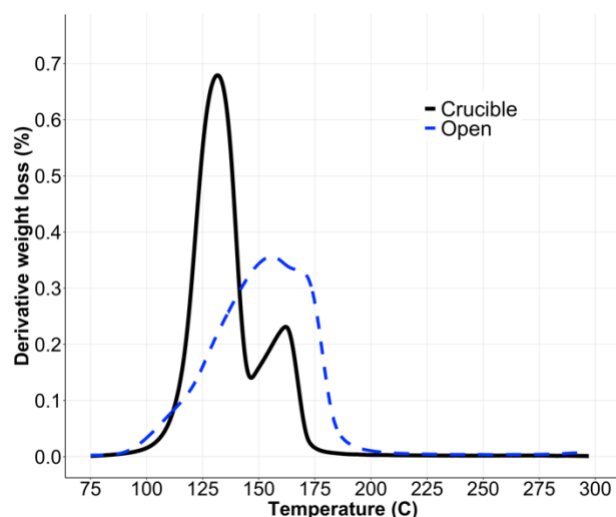


Figure 54. Cellulose-gypsum composite DTG curve comparison with a crucible (black) and without (blue)

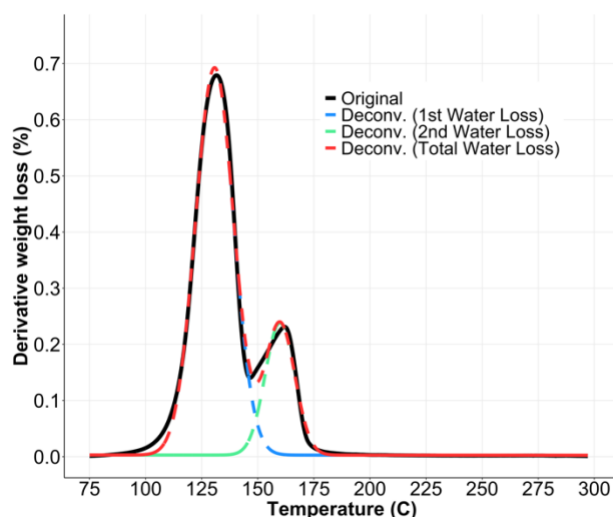


Figure 55. DTG curves: original (black), deconvoluted 1st water loss (blue), deconvoluted 2nd water loss (green), deconvoluted total loss (red)

To separate the overlapping chemical processes, a mathematical procedure based on peak deconvolution using the Frazer-Suzuki statistical function was applied to all DTG thermal curves as shown in Figure 55. This novel approach based on peak convolution has become common in literature alongside other functions such as Gaussian and Lorentzian<sup>24</sup>. The Frazer-Suzuki function was chosen due to its asymmetrical deconvolution capabilities of complex processes<sup>24</sup>. The function can be expressed as follows:

$$y = a_0 e \left[ -\ln 2 \left( \frac{1}{a_3} \ln \left( 1 + 2a_3 \frac{x - a_1}{a_2} \right) \right)^2 \right] \quad \begin{array}{l} \text{Equation 16.} \\ \text{Frazer-Suzuki function}^{24} \end{array}$$

Where  $a_0$ ,  $a_1$ ,  $a_2$ , and  $a_3$  are amplitude, position, half width and shape (asymmetry) of the curve respectively<sup>24,75</sup>. Deconvolution was applied for only the two peaks of water loss and the resulting curves were integrated to amount the mass loss. Fityk curve fitting software was used for deconvolution with addition of a user defined function due to Frazer-Suzuki not being one of the provided statistical functions. RStudio software was used for plotting.

## 4.4 Results and Discussion

### 4.4.1 Compressive Strength

Compressive strengths calculated from the uniaxial compression data are illustrated in Table 7. In Figure 56, when adding cellulose nanocrystals (CNC) to plaster of Paris (p.o.P) and water, the CNC-gypsum composites either maintained or increase compressive strength. As for cellulose nanofibrils (CNF), compressive strength changes were inconsistent across all w/b ratios. Looking at samples with the highest w/b ratio (1:1.5) in Figure 57, CNF maintained compressive strength expect for at the highest concentration tested (1% CNF) where it increased compressive strength similar to CNC highest concentration tested (3.33% CNC). It appears to be that the concentration threshold to improve compressive strength is lower for CNC but a similar improvement can be achieved with CNF at a lower concentrations. This could be due to CNC's smaller dimension requiring lower concentrations than CNF to initiate compressive strength improvement but CNF requiring lower concentration than CNC to reach similar compressive

strength improvements. A similar trend is demonstrated with the lower w/b ratios 1:2 and 1:2.5 in Figure 58 and Figure 59 respectively. For the 1:2 w/b ratio, CNC addition improved compressive strength a lower concentration than CNF and the concentration for CNF to improve compressive strength was not reached from the profiles tested. As for the 1:2.5 w/b ratio, both CNC and CNF improved compressive strength for all concentrations tested. Decreasing the w/b ratio increases mechanical performance as gypsum's mechanical performance is correlated to its total porosity such that lower porosity results from a lower w/b ratio as clearly demonstrated in Figure 60<sup>71</sup>.

In Figure 61, compressive strength is plotted against cellulose nanomaterial (CNM) concentration. Once again, lower w/b ratio results in higher compressive strength and each ratio is differentiated by color and each CNM is differentiated by a solid line for CNC and dashed line for CNF. This plot also demonstrates the cross-over between CNC and CNF for the highest 1:1.5 w/b ratio that was described for Figure 57. Overall, adding either CNM at low concentration (~ 14%) improve mechanical properties. The improvements in strength can be attributed to the CNM's high tensile strength and Young's modulus that could affect the gypsum network entanglement as seen in other research<sup>71</sup>.

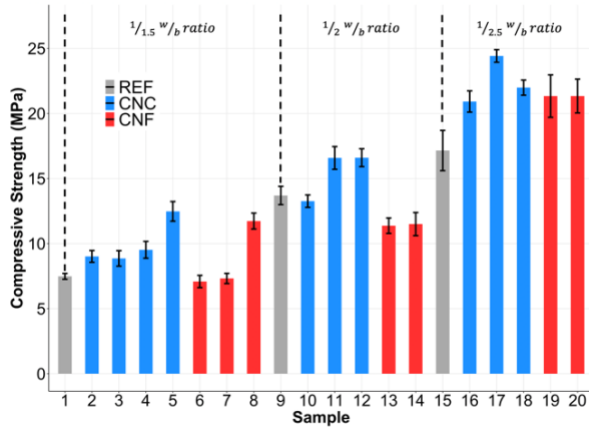


Figure 56. Compressive strength for cellulose-gypsum composites across three w/b ratios

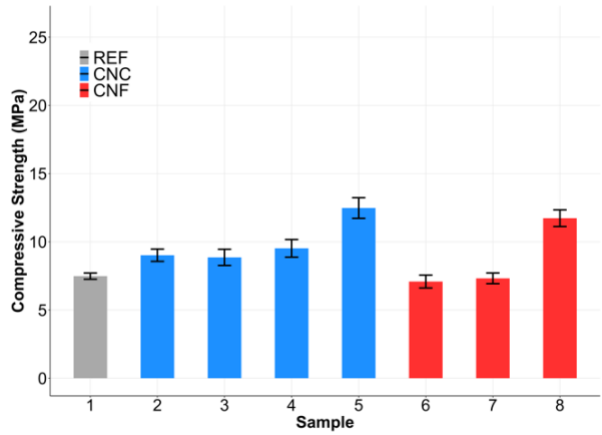


Figure 57. Compressive strength for cellulose-gypsum composites with 1:1.5 b/w ratio

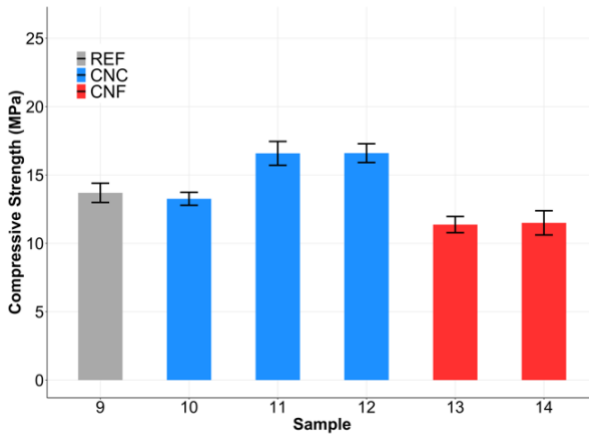


Figure 58. Compressive strength for cellulose-gypsum composites with 1:2 w/b ratio

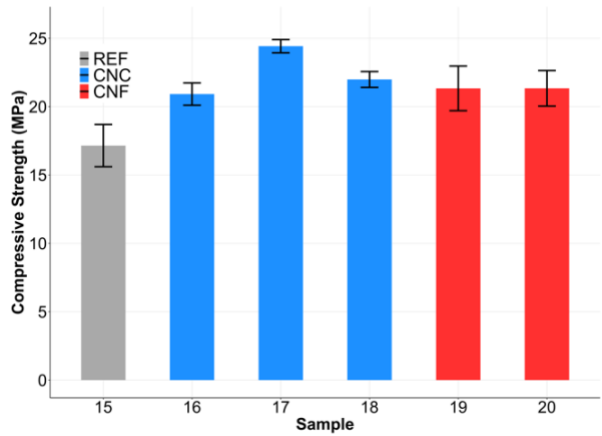


Figure 59. Compressive strength for cellulose-gypsum composites with 1:2.5 w/b ratio

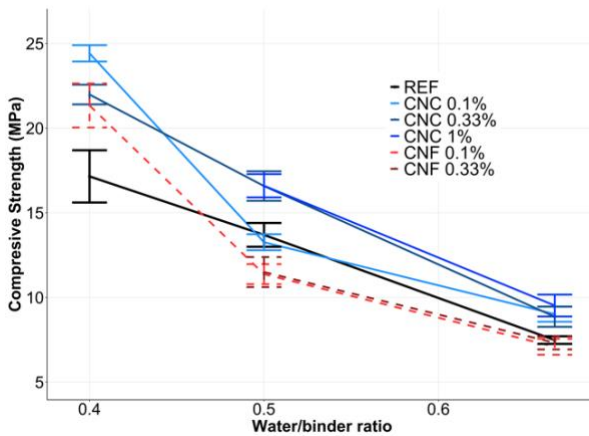


Figure 60. Binder/water ratio dependence for the following concentrations: 0% (REF), 0.1% CNC, 0.33% CNC, 1% CNC, 0.1% CNF, 0.33% CNF

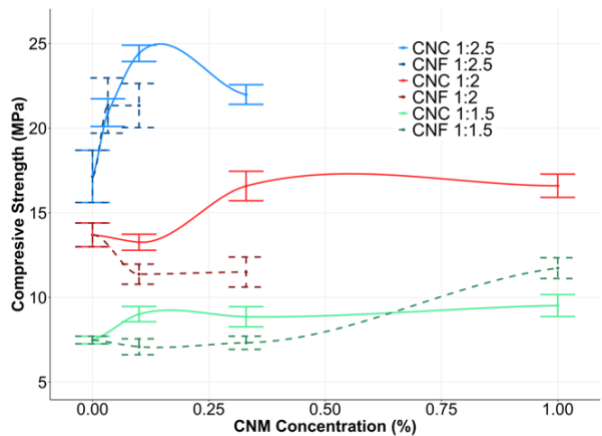


Figure 61. Compressive Strength CNC/CNF concentration dependence for all profiles except profile no. 5 (CNC 3.33wt%, 1:2.5 w/b ratio)

#### 4.4.2 Thermogravimetric Analysis (TGA)

TGA derivative thermogravimetric curve (DTG) curves representing mass losses and their respective total mass losses are illustrated in **Error! Reference source not found.** In Figure 62, all cellulose-gypsum composite profiles with a 1:1.5 w/b ratio are plotted with CNC profiles as dashed lines and CNF as dotted lines. The first observation is the subtle appearance of an additional mass loss bump after 225 °C that is due to the small concentration of added cellulose nanomaterials (CNM). It is most prominent with the highest CNC concentration of 3.33% (yellow dashed line) where at approximately 238 °C that CNC starts to degrade as reflected in literature<sup>76</sup>. The second observation is the shift in peaks for the overlapping dehydrations when introducing CNM. When introducing CNC, there is not consistent trend occurring as concentration increases but for the highest concentration of 3.33% there are shifts; the gap between the two peaks widens by the first peaks slight shifting left and the second shifting right. As for adding CNF, there is an opposing trend where increasing concentration shortens the gap between peaks whereas the first peak stays relatively the same and the second peak shifts left with increasing concentration. This could indicate CNC and CNF are delaying and accelerating hydration of the second water loss in gypsum but needs further investigation. In Figure 63, for the cellulose-gypsum composite profiles with a 1:2 w/b ratio, both observations of a subtle third peak and the widening and shrinking of the gap due to CNC and CNF addition respectively are also illustrated. As for Figure 64, the two previously mentioned observations were not strongly present and could be due to the 1:2.5 w/b ratio that calls for less water being used resulting in less dispersion of the CNM throughout the mixture<sup>70</sup>. In Figure 65, total mass loss (area under the curve) due to dehydration of all cellulose gypsum composites is plotted with an average of 19.48% ± 1.5% indicating no significant changes due to the small range. According to literature and stoichiometry, the theoretical mass loss of water in pure gypsum is 20.9%<sup>24,25</sup>. Taking the average total loss and dividing by the theoretical 20.9% for pure gypsum results in a 93.21% degree of purity which may be the reason for the difference between the resulting average and theoretical value<sup>20,22</sup>.

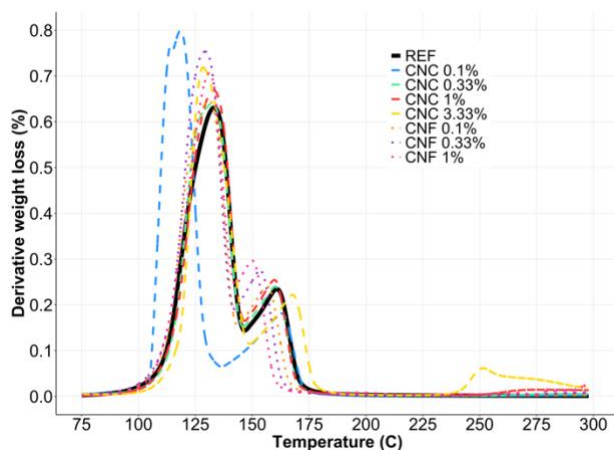


Figure 62. Cellulose-gypsum composite DTG curves for all 1:1.5 w/b ratio profiles (1-7 legend top to bottom)

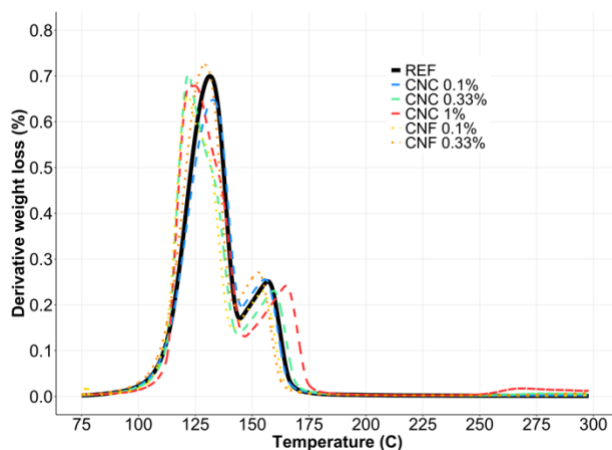


Figure 63. Cellulose-gypsum composite DTG curves for all 1:2 w/b ratio profiles (8-13 legend top to bottom)

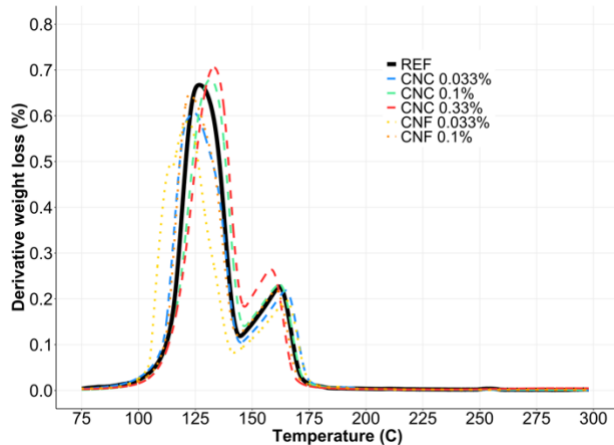


Figure 64. Cellulose-gypsum composite DTG curves for all 1:2.5 w/b ratio profiles (14-20 legend top to bottom)

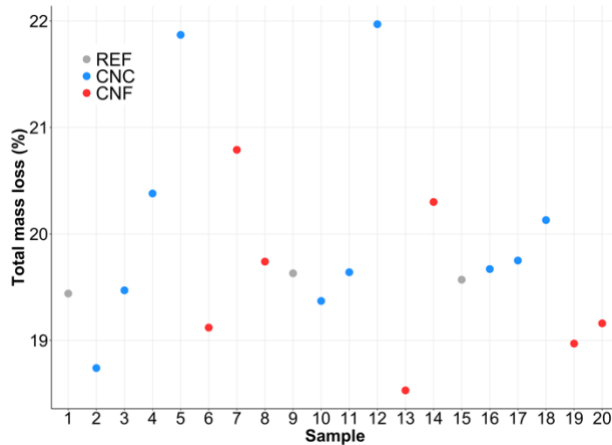


Figure 65. Cellulose-gypsum composite total mass losses

**Error! Reference source not found.** demonstrates the mass loss curves resulting from Frazer-Suzuki deconvolution where figures on the left illustrate the two separated water mass losses (A and B) for each profile and figures on the right are the summation of A and B curves for each profile. Although the overlapping reactions were able to be mathematically separated, there still is an overlap between the two dehydration steps. They also do not reflect the theoretical water mass losses of 15.7%, 5.2% and 20.9% for the first, second and total water loss respectively possibly due to the non-100% gypsum purity previously mentioned and the fact that Frazer-Suzuki deconvolution uses mathematical estimation to separate the complex overlapping reactions<sup>24,25</sup>.

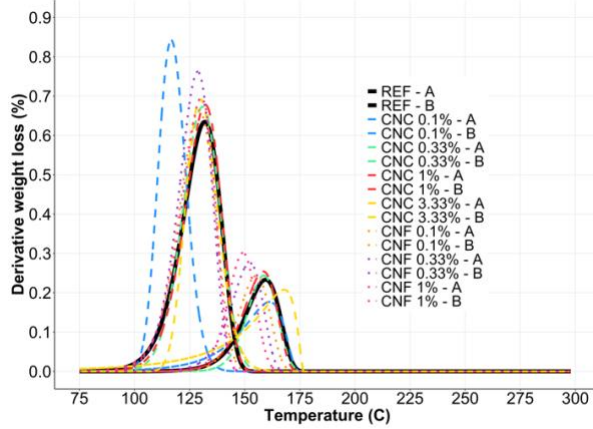


Figure 66. Deconvolved cellulose-gypsum composite DTG curves for all 1:1.5 w/b ratio profiles

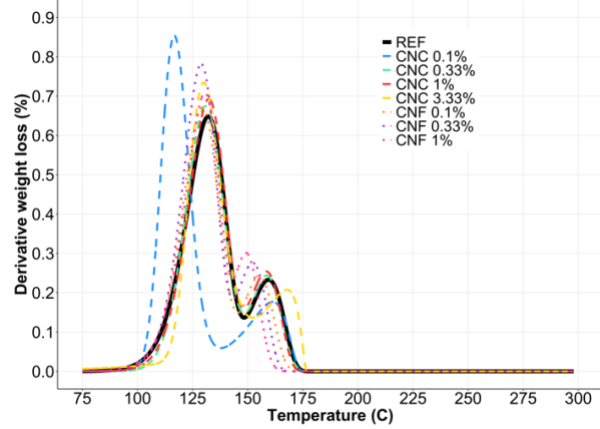


Figure 67. Deconvolved total cellulose-gypsum composite DTG curves for all 1:1.5 w/b ratio profiles

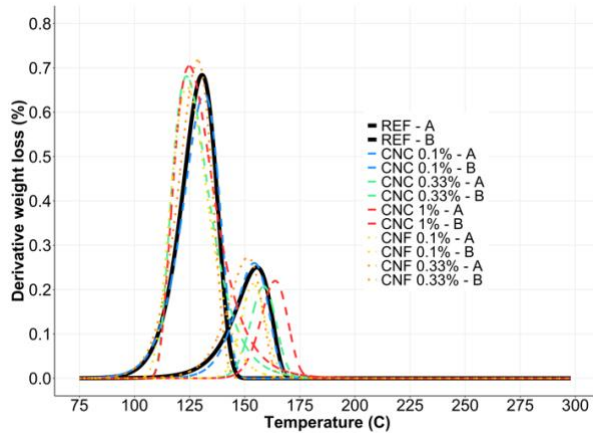


Figure 68. Deconvolved cellulose-gypsum composite DTG curves for all 1:2 w/b ratio profiles

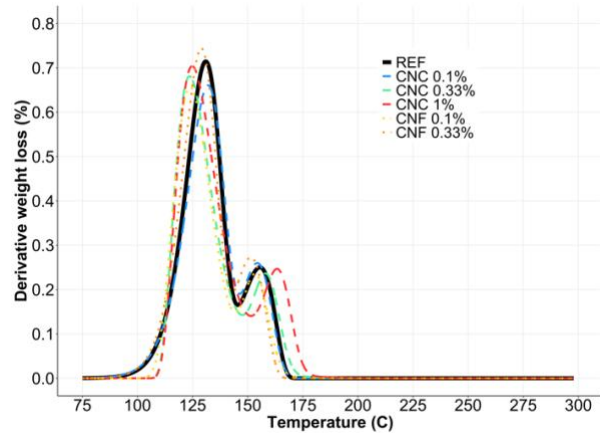


Figure 69. Deconvolved total cellulose-gypsum composite DTG curves for all 1:2 w/b ratio profiles

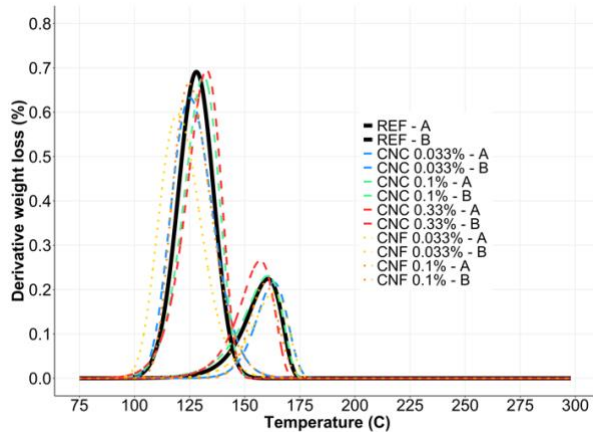


Figure 70. Deconvolved cellulose-gypsum composite DTG curves for all 1:2.5 w/b ratio profiles

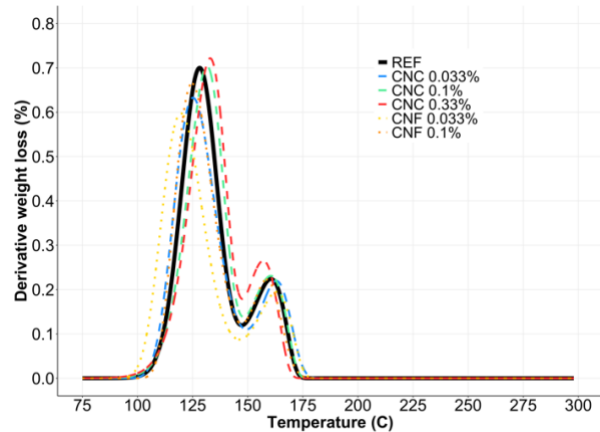


Figure 71. Deconvolved total cellulose-gypsum composite DTG curves for all 1:2.5 w/b ratio profiles

## 4.5 Conclusions

Two cellulose nanomaterials (cellulose nanocrystals and cellulose nanofibrils) were used in this chapter to investigate the influence on mechanical properties when combined with plaster of Paris and water in the making of gypsum. Thermalgravimetric analysis was also completed. The conclusion is as followed:

- As expected, lower water-to-binder ratio increases gypsum's compressive strength was confirmed due to lower dispersion and lower total porosity
- Adding CNC at low concentrations (0.1 - 1%) either maintained or increased gypsum's compressive strength
- Adding CNF at low concentrations (0.1 - 1%) initially slightly decreased in gypsum's compressive strength at lower concentrations and increased at higher concentrations. This could be due to CNF's larger dimensions requiring higher concentrations than CNC in order to initiate compressive strength improvement but needs further investigating
- Adding CNF required a lower concentration than that of CNC for similar compressive strength improvements. This could be due to CNF's larger dimensions being more efficient of a structural nanomaterial than CNC but needs further investigating
- Generally, adding CNC or CNF at low concentrations (0.1 - 1%) can improve gypsum's compressive strength
- Thermogravimetric analysis of gypsum requires use of a crucible with pinhole lid to separate the two overlapping dehydration reactions
- Adding CNC and CNF at low concentrations (0.1 - 1%) resulting in a widening and shrinking of the gap between the 1<sup>st</sup> and 2<sup>nd</sup> peak respectively representing water loss steps
- Deconvolution can be applied to mathematically separate the overlapping dehydration reactions in gypsum but considering the chemical decompositions are complex such estimations should be completed with caution

## 5. CONCLUSION

### 5.1 Summary

The problem lies within cement production's contribution to global CO<sub>2</sub> emissions as significant research efforts have demonstrated that nanomaterials as an additive are becoming an effective solution. Cellulose nanocrystals (CNC) are a sustainable material that improve cement performance resulting in less being produced. Bridging CNC and cement for industry implementation will come from CNC and cement interaction knowledge development as investigated in this study. Four CNCs and four cements were used to investigate the effect on the resistance to chloride ingress for cement with CNC as an additive through formation factor methodology. Formation factor is a transport property that has great potential for replacing RCPT but still needs further development. Two cellulose nanomaterials (cellulose nanocrystals and cellulose nanofibrils) were used to investigate the influence on mechanical properties when combined with plaster of Paris and water in the making of gypsum. Thermalgravimetric analysis was also completed. The continuous, intensive research on cellulose nanomaterials applications in cement has gained great momentum and benchmarks to eventually create a low-cost, sustainable material that will be implemented into industry production processes to create a new series of commercial cellulose-cement composites with improved performance with less material.

### 5.2 Conclusions

The conclusions are summarized as follows:

#### Effect of CNC on formation factor

- Resistance and formation factor gradually increase over time due to ongoing hydration
- CNC addition to cement at small concentrations (0.2 – 0.5%) does not always improve resistance and formation factor and is dependent on cement type and CNC source material
- Of the CNCs and OPCs used, a significant increase in formation factor over time was demonstrated when CNC was combined with Type V OPC
- Higher water-to-cement ratios reduced formation factor value ranges and can be attributed to the increase in water resulting in greater dispersion and lower formation factor

- OPC Type III B and Type V demonstrated a significant increase in formation factor at early ages when CNC was added
- OPC Type V with a water-to-cement ratio of 0.3 demonstrated a significant increase in formation factor for both early and late ages when CNC was added
- OPC Type I/II with a water-to-cement ratio of 0.3 demonstrated a significant increase in formation factor for late age when CNC was added
- Using the Nernst-Einstein relationship and Fick's second law, a life-cycle estimation for chloride ingress can be calculated using a diffusion-based model

#### Effect of CNC/CNF on mechanical properties and thermal analysis

- Lower water-to-binder ratio increases gypsum's compressive strength due to lower dispersion and lower total porosity
- Adding CNC at low concentrations (0.1 - 1%) either maintained or increased gypsum's compressive strength
- Adding CNF at low concentrations (0.1 - 1%) initially decreased in gypsum's compressive strength at lower concentrations and increased at higher concentrations.
- Adding CNF required a lower concentration than that of CNC for similar compressive strength improvements.
- Generally, adding CNC or CNF at low concentrations (0.1 - 1%) improve gypsum's compressive strength
- Thermogravimetric analysis of gypsum requires use of a crucible with pinhole lid to separate the two overlapping dehydration reactions
- Adding CNC and CNF at low concentrations (0.1 - 1%) results in a widening and shrinking of the gap between the 1<sup>st</sup> and 2<sup>nd</sup> water loss peaks respectively
- Deconvolution can mathematically separate overlapping reactions but considering the overlapping reactions are complex such estimations should be completed with caution

### 5.3 Future Work

The following are recommendations for future work as it relates to the influence of cellulose nanocrystals on performance and transport properties of cementitious materials and gypsum:

- For the formation factor experiment, completing mechanical testing via Ball-On-Three-Ball (B3B) testing to measure flexural strength or completing compressive strength testing for comparison to formation factor data
- For the formation factor experiment, completing porosity characterization via BET specific surface area analysis or ASTM C642, Standard Test Method for Density, Absorption, and Voids in Hardened Concrete
- For the formation factor experiment, completing imaging slices of cylinder sample to analyze the CNC and cement interactions
- For the gypsum experiment, further investigate Frazer-Suzuki function parameter optimization for best deconvolved dehydration curves
- Investigate the influence of CNC size on the formation factor of cement paste via size separation filter experiments will be conducted. CNC surface chemistry should also be analyzed by using different CNC profiles to filter
- Investigate the effect of cement age at which CNC is added has on formation factor

## APPENDIX A: NOMENCLATURE

Equation	Description (Units)
Equation 5	$C_{x,t}$ chloride concentration at time $t$ (seconds) at depth $x$ (meters) (% by mass of concrete)
	$C_0$ background chloride concentration (% by mass of concrete)
	$C_s$ chloride concentration at the surface (% by mass of concrete)
	$D_a$ apparent chloride diffusion coefficient (meter <sup>2</sup> /second)
	$erfc(y)$ complimentary error function of $y$
Equation 6	$\Omega$ ohms
	$\rho$ resistivity ( $\Omega \cdot$ meters)
	$R$ resistance ( $\Omega$ )
	$k$ geometry correction factor (unitless)
Equation 7	$D_i$ diffusivity of ion $i$ (meter <sup>2</sup> /second)
	$\sigma_i$ the partial conductivity of ion $i$ (Siemens/meter)
	$R$ gas constant (8,314 Joules/mole)
	$T$ absolute temperature (K)
	$Z_i$ charge of ion $i$
	$F$ Faraday's constant (96500 Coulombs/mole)
	$C_i$ concentration of ion $i$ (mol/m <sup>2</sup> )

Equation		Description (Units)
Equation 8	$Q_{RCPT}$	RCPT total charged passed (Coulombs)
	$I$	current (amps)
	$V$	voltage (volts)
	$L$	length (meters)
	$A$	cross sectional area of the sample (meters <sup>2</sup> )
	$t$	test time (hours)
Equation 9	$F$	formation factor (unitless)
	$\rho$	bulk resistivity ( $\Omega \cdot$ meters)
	$\rho_o$	pore solution resistivity ( $\Omega \cdot$ meters)
	$\beta$	tortuosity (unitless)
	$\varphi$	porosity (unitless)
Equation 11	$R_{cylinder}$	resistance of the sample ( $\Omega$ )
	$R_{measured}$	resistance including the conductivity media ( $\Omega$ )
	$R_{top\ sponge}$	resistance of top conductive medium ( $\Omega$ )
	$R_{bottom\ sponge}$	resistance of bottom conductive medium ( $\Omega$ )
Equation 13	$SE$	standard error (units of data)
Equation 15	$\sigma$	sample standard deviation (units of data)
	$n$	number of samples

---

<b>Equation</b>		<b>Description (Units)</b>
	$a_0$	amplitude
Equation 16	$a_1$	position
	$a_2$	half width
	$a_3$	shape/asymmetry

---

## APPENDIX B: ACRONYMS

---

	<b>Definition</b>
ACI	American Concrete Institute
ASTM	American Society for Testing and Materials
AASHTO	American Association of State Highway and Transportation Officials
BGB	Blue Goose Biorefineries
B3B	Ball on 3 Ball mechanical testing
CNC	Cellulose Nanocrystals
CNF	Cellulose Nanofibrils
CNM	Cellulose Nanomaterials
DI	De-Ionized
DOH	Degree of Hydration
DT	Destructive Testing
DTG	Derivative Thermogravimetry curve
FPL	Forest Products Laboratory
HPC	High-performance concrete
NDT	Non-Destructive Testing
OPC	Ordinary Portland Cement
OSU	Oregon State University

---

<b>Definition</b>	
RCPT	Rapid Chloride Permeability Test
SCD	Short Circuit Diffusion
SCM	Supplementary Cementitious Materials
TGA	Thermogravimetric Analysis
WRA	Water Reducing Admixture

---

## REFERENCES

- (1) Andrew, R. M. Global CO<sub>2</sub> Emissions from Cement Production. *Earth Syst. Sci. Data* **2018**, *10* (1), 195–217. <https://doi.org/10.5194/essd-10-195-2018>.
- (2) Hannah Ritchie; Max Roser. CO<sub>2</sub> and Greenhouse Gas Emissions. *Our World Data* **2020**. <https://doi.org/10.5194/ESSDD-2017-123>.
- (3) Kosmatka SH, Panarese WC, K. B. *Design and Control Design and Control of Concrete Mixtures*; 2002.
- (4) Moon, R. J.; Martini, A.; Nairn, J.; Simonsen, J.; Youngblood, J. Cellulose Nanomaterials Review: Structure, Properties and Nanocomposites. *Chem. Soc. Rev.* **2011**, *40* (7), 3941–3994. <https://doi.org/10.1039/c0cs00108b>.
- (5) Fu, T.; Montes, F.; Suraneni, P.; Youngblood, J.; Weiss, J. The Influence of Cellulose Nanocrystals on the Hydration and Flexural Strength of Portland Cement Pastes. *Polymers (Basel)*. **2017**, *9* (9). <https://doi.org/10.3390/polym9090424>.
- (6) Basheer, L.; Kropp, J.; Cleland, D. J. Assessment of the Durability of Concrete from Its Permeation Properties: A Review. *Constr. Build. Mater.* **2001**. [https://doi.org/10.1016/S0950-0618\(00\)00058-1](https://doi.org/10.1016/S0950-0618(00)00058-1).
- (7) Gupta, S. Comparison of Non-Destructive and Destructive Testing on Concrete: A Review. *Trends Civ. Eng. its Archit.* **2018**, *3* (1). <https://doi.org/10.32474/tceia.2018.03.000154>.
- (8) Verma, S. K.; Bhadauria, S. S.; Akhtar, S. Review of Nondestructive Testing Methods for Condition Monitoring of Concrete Structures. *J. Constr. Eng.* **2013**, *2013*, 1–11. <https://doi.org/10.1155/2013/834572>.
- (9) Jason Weiss, W.; Spragg, R. P.; Burkan Isgor, O.; Tyler Ley, M.; Van Dam, T. Toward Performance Specifications for Concrete: Linking Resistivity, RCPT and Diffusion Predictions Using the Formation Factor for Use in Specifications. In *High Tech Concrete: Where Technology and Engineering Meet - Proceedings of the 2017 fib Symposium*;

- Springer International Publishing, 2017; pp 2057–2065. [https://doi.org/10.1007/978-3-319-59471-2\\_235](https://doi.org/10.1007/978-3-319-59471-2_235).
- (10) Flores, J.; Kamali, M.; Ghahremaninezhad, A.; Flores, J.; Kamali, M.; Ghahremaninezhad, A. An Investigation into the Properties and Microstructure of Cement Mixtures Modified with Cellulose Nanocrystal. *Materials (Basel)*. **2017**, *10* (5), 498. <https://doi.org/10.3390/ma10050498>.
- (11) Kim, J. H.; Shim, B. S.; Kim, H. S.; Lee, Y. J.; Min, S. K.; Jang, D.; Abas, Z.; Kim, J. Review of Nanocellulose for Sustainable Future Materials. *International Journal of Precision Engineering and Manufacturing - Green Technology*. Korean Society for Precision Engineering April 1, 2015, pp 197–213. <https://doi.org/10.1007/s40684-015-0024-9>.
- (12) Fu, T.; Moon, R. J.; Zavattieri, P.; Youngblood, J.; Weiss, W. J. Cellulose Nanomaterials as Additives for Cementitious Materials. *Cellul. Nanofibre Compos.* **2017**, 455–482. <https://doi.org/10.1016/B978-0-08-100957-4.00020-6>.
- (13) Thomas, M.; Tennis, P. *Cements for Use in Concrete, CD050*.
- (14) J. Olek. CE 597 Purdue Sustainable Binders Course.
- (15) Malek, J.; Kaouther, M. Destructive and Non-Destructive Testing of Concrete Structures. *Jordan J. Civ. Eng.* **2014**, *8* (4), 432–441.
- (16) Mehta, P. K. (Povindar K.; Monteiro, P. J. M. *Concrete : Microstructure, Properties, and Materials*; McGraw-Hill Education: New York, Chicago, San Francisco, Athens, London, Madrid, Mexico City, Milan, New Delhi, Singapore, Sydney, Toronto, 2014.
- (17) Cao, Y. Nano-Modification for High Performance Cement Composites with Cellulose NanoCrystals and Carbon Nanotubes. *Open Access Diss.* **2014**.
- (18) Feng, X.; Garboczi, E. J.; Bentz, D. P.; Stutzman, P. E.; Mason, T. O.; Feng, X.; Garboczia, E. J.; Bentza, D. P.; Stutzmana, P. E.; Masonb, T. O. *Estimation of the Degree of Hydration of Blended Cement Pastes by a Scanning Electron Microscopy Point-Counting Procedure*;

2004; Vol. 34.

- (19) Sun, X.; Wu, Q.; Lee, S.; Qing, Y.; Wu, Y. Cellulose Nanofibers as a Modifier for Rheology, Curing and Mechanical Performance of Oil Well Cement. *Sci. Rep.* **2016**, *6*. <https://doi.org/10.1038/srep31654>.
- (20) Dweck, J.; Leonardo, R. S.; Cartledge, F. K.; Mendoza Reales, O. A.; Toledo Filho, R. D. Gypsum Content Determination in Portland Cements by Thermogravimetry. *J. Therm. Anal. Calorim.* **123**. <https://doi.org/10.1007/s10973-015-5078-y>.
- (21) Javangula, H. *Comparative Studies On Standard and Fire-Rated Gypsum Wallboards*; 2014.
- (22) Borrachero, M. V.; Payá, J.; Bonilla, M.; Monzó, J. The Use of Thermogravimetric Analysis Technique for the Characterization of Construction Materials: The Gypsum Case. *J. Therm. Anal. Calorim.* **2008**, *91* (2), 503–509. <https://doi.org/10.1007/s10973-006-7739-3>.
- (23) Elena Charola Josef Pühringer AE Michael Steiger, A. A. Gypsum: A Review of Its Role in the Deterioration of Building Materials. <https://doi.org/10.1007/s00254-006-0566-9>.
- (24) El Hazzat, M.; Sifou, A.; Arsalane, S.; El Hamidi, A. Novel Approach to Thermal Degradation Kinetics of Gypsum: Application of Peak Deconvolution and Model-Free Isoconversional Method. *J. Therm. Anal. Calorim.* **2020**, *140* (2), 657–671. <https://doi.org/10.1007/s10973-019-08885-3>.
- (25) *Materials Characterization by Thermal Analysis (DSC & TGA), Rheology, and Dynamic Mechanical Analysis Charles Potter-Thermal Application Scientist Sarah Cotts-Rheology Application Scientist Fred Wiebke-Territory Manager © TA Instruments.*
- (26) Mettler Toledo. *Determination of Calcium Sulfate Dihydrate and Hemihydrate in Cement*; 2010.
- (27) Czaderna, A.; Kocemba, A.; Kozanecki, M.; Mucha, M.; Mróz, P. The Influence of Cellulose Derivatives on Water Structure in Gypsum. *Constr. Build. Mater.* **2018**, *160*, 628–638. <https://doi.org/10.1016/j.conbuildmat.2017.11.062>.

- (28) Azarsa, P.; Gupta, R. Electrical Resistivity of Concrete for Durability Evaluation: A Review. *Adv. Mater. Sci. Eng.* **2017**, *2017*, 1–30. <https://doi.org/10.1155/2017/8453095>.
- (29) Claisse, P. *Transport Properties of Concrete*.
- (30) Whatley, S. A Comparison of Formation Factor to Standard Methods to Evaluate Transport Properties. **2018**.
- (31) Bu, Y.; Luo, D.; Weiss, J. Advances in Civil Engineering Materials Using Fick's Second Law and Nernst-Planck Approach in Prediction of Chloride Ingress in Concrete Materials. **2014**. <https://doi.org/10.1520/ACEM20140018>.
- (32) Arias, W. J. *BULK DIFFUSION OF HIGH PERFORMANCE CONCRETE SPECIMENS EXPOSED TO DIFFERENT LEVELS OF SODIUM CHLORIDE AND SEAWATER*; 2014.
- (33) Weiss, W. J.; Burkan Isgor, O. *Examining How Saturation and Pore Solution Chemistry Impact Durability Test Methods, Specifications and Service Life Models (Keynote)*.
- (34) Chaudhry, R. H. Determination of Air Voids , Capillary , and Gel Porosity in Hardened Concrete Using Mass-Based Saturation Techniques. **2018**.
- (35) Mehta, P. K. (Povindar K. *Concrete: Structure, Properties and Materials*; 1986; Vol. 8. [https://doi.org/10.1016/0262-5075\(86\)90055-2](https://doi.org/10.1016/0262-5075(86)90055-2).
- (36) Correia, C. de M. P.; de Souza, M. F. Mechanical Strength and Thermal Conductivity of Low-Porosity Gypsum Plates. *Mater. Res.* **2009**, *12* (1), 95–99. <https://doi.org/10.1590/S1516-14392009000100012>.
- (37) Tonoli, G. H. D.; Rodrigues Filho, U. P.; Savastano, H.; Bras, J.; Belgacem, M. N.; Rocco Lahr, F. A. Cellulose Modified Fibres in Cement Based Composites. *Compos. Part A Appl. Sci. Manuf.* **2009**. <https://doi.org/10.1016/j.compositesa.2009.09.016>.
- (38) Ardanuy, M.; Claramunt, J.; Arévalo, R.; Parés, F.; Aracri, E.; Vidal, T. *NFC/Cement Mortar Composites*; 2012; Vol. 7.
- (39) Microfibrillated cellulose, a new cellulose product: properties, uses, and commercial

- potential (Conference) | OSTI.GOV <https://www.osti.gov/biblio/5062478> (accessed Oct 29, 2020).
- (40) Cao, Y.; Tian, N.; Bahr, D.; Zavattieri, P. D.; Youngblood, J.; Moon, R. J.; Weiss, J. The Influence of Cellulose Nanocrystals on the Microstructure of Cement Paste. *Cem. Concr. Compos.* **2016**, *74*. <https://doi.org/10.1016/j.cemconcomp.2016.09.008>.
- (41) Cao, Y.; Zavatterri, P.; Youngblood, J.; Moon, R.; Weiss, J. The Influence of Cellulose Nanocrystal Additions on the Performance of Cement Paste. *Cem. Concr. Compos.* **2015**, *56*. <https://doi.org/10.1016/j.cemconcomp.2014.11.008>.
- (42) Medeiros, R. A.; Lima, M. G. Electrical Resistivity of Unsaturated Concrete Using Different Types of Cement. *Constr. Build. Mater.* **2016**. <https://doi.org/10.1016/j.conbuildmat.2015.12.168>.
- (43) AASHTO TP 119, “Standard Method of Test for Electrical Resistivity of a Concrete Cylinder Tested in a Uniaxial Resistance Test.” American Association of State Highway and Transportation Officials: Washington DC 2017, p 14 pp.
- (44) Sant, G.; Bentz, D.; Weiss, J. Capillary Porosity Depercolation in Cement-Based Materials: Measurement Techniques and Factors Which Influence Their Interpretation. *Cem. Concr. Res.* **2011**, *41*, 854–864. <https://doi.org/10.1016/j.cemconres.2011.04.006>.
- (45) Tanesi, J.; Montanari, L.; Ardani, A. *Formation Factor Demystified and Its Relationship to Durability*; 2019.
- (46) ASTM C1202. Standard Test Method for Electrical Indication of Concrete’s Ability to Resist Chloride Ion Penetration. *Am. Soc. Test. Mater.* **2012**, No. C, 1–8. <https://doi.org/10.1520/C1202-12.2>.
- (47) GCP. *Introduction How and Why Was This Test Method Developed? Understanding AASHTO T277 and ASTM C1202 Rapid Chloride Permeability Test*; 2016.
- (48) Stanish, K. D.; Hooton, R. D.; Thomas, M. D. . *Testing the Chloride Penetration Resistance of Concrete : A Literature Review*; 1997.

- (49) Spragg, R. P.; Bu, Y.; Snyder, K. A.; Bentz, D. P.; Weiss, J. *Electrical Testing of Cement-Based Materials: Role of Testing Techniques, Sample Conditioning, and Accelerated Curing*; Joint Transportation Research Program, Indiana Department of Transportation, and Purdue University, 2013. <https://doi.org/10.5703/1288284315230>.
- (50) Shi, C. Effect of Mixing Proportions of Concrete on Its Electrical Conductivity and the Rapid Chloride Permeability Test (ASTM C1202 or ASSHTO T277) Results. *Cem. Concr. Res.* **2004**. <https://doi.org/10.1016/j.cemconres.2003.09.007>.
- (51) What is formation factor and why should we care about it? <https://www.linkedin.com/pulse/what-formation-factor-why-should-we-care-milena-rangelov-ph-d-> (accessed Jul 18, 2019).
- (52) Spragg, R.; Villani, C.; Weiss, J. Electrical Properties of Cementitious Systems: Formation Factor Determination and the Influence of Conditioning Procedures. *Adv. Civ. Eng. Mater.* **2016**, 5 (1), 20150035. <https://doi.org/10.1520/ACEM20150035>.
- (53) Spragg, R.; Qiao, C.; Barrett, T.; Weiss, J. Assessing a Concrete's Resistance to Chloride Ion Ingress Using the Formation Factor. In *Corrosion of Steel in Concrete Structures*; 2016. <https://doi.org/10.1016/B978-1-78242-381-2.00011-0>.
- (54) Designation: C1556 – 11a Standard Test Method for Determining the Apparent Chloride Diffusion Coefficient of Cementitious Mixtures by Bulk Diffusion 1. <https://doi.org/10.1520/C1556-11AR16>.
- (55) Moradillo, M. K.; Qiao, C.; Isgor, B.; Reese, S.; Weiss, W. J. Relating Formation Factor of Concrete to Water Absorption. *ACI Mater. J.* **2018**, 115 (6), 887–898. <https://doi.org/10.14359/51706844>.
- (56) Weiss, J. *Performance Specifications and Durability Slides Prepared by Jason Weiss Slide 1 of 32 Durability in Concrete: Toward Performance Specifications*; 2016.
- (57) Tsui-Chang, M.; Suraneni, P.; Montanari, L.; Muñoz, J. F.; Jason Weiss, W. Determination of Chemical Composition and Electrical Resistivity of Expressed Cementitious Pore Solutions Using X-Ray Fluorescence. *ACI Mater. J.* **2019**, 116 (1), 155–164.

<https://doi.org/10.14359/51712242>.

- (58) Snyder, K. A.; Feng, X.; Mason, T. O. Estimating the Electrical Conductivity of Cement Paste Pore Solutions from OH<sup>-</sup>, K<sup>+</sup> and Na<sup>+</sup> Concentrations | NIST. *Cem. Concr. Res.* **2003**, *33* (6).
- (59) Kurdowski, W. *Cement and Concrete Chemistry*; Springer Netherlands: Dordrecht, 2014. [https://doi.org/10.1007/978-94-007-7945-7\\_6](https://doi.org/10.1007/978-94-007-7945-7_6).
- (60) Hussain, S.; Bhunia, D.; Singh, S. B. An Experimental Investigation of Accelerated Carbonation on Properties of Concrete. *Eng. J.* **2016**, *20* (2), 29–38. <https://doi.org/10.4186/ej.2016.20.2.29>.
- (61) Tabsh, S. W.; Abdelfatah, A. S. Influence of Recycled Concrete Aggregates on Strength Properties of Concrete. *Constr. Build. Mater.* **2009**. <https://doi.org/10.1016/j.conbuildmat.2008.06.007>.
- (62) Naghibdehi, M. G.; Naghipour, M.; Rabiee, M. Behaviour of Functionally Graded Reinforced-Concrete Beams under Cyclic Loading. *Gradjevinar* **2015**, *67* (5). <https://doi.org/10.14256/JCE.1124.2014>.
- (63) Yao, W.; Jiang, S.; Fei, W.; Cai, T. Correlation between the Compressive, Tensile Strength of Old Concrete under Marine Environment and Prediction of Long-Term Strength. *Adv. Mater. Sci. Eng.* **2017**, *2017*. <https://doi.org/10.1155/2017/8251842>.
- (64) ASTM. ASTM C150 / C150M-19a Standard Specification for Portland Cement <http://www.astm.org/cgi-bin/resolver.cgi?C150C150M> (accessed Oct 29, 2020).
- (65) Reiner, R. S.; Rudie, A. W. *Production and Applications of Cellulose Nanomaterials 1.1 Preparation and Characterization Process Scale-Up of Cellulose Nanocrystal Production to 25 Kg per Batch at the Forest Products Laboratory*; 2013.
- (66) (1) Why do we test concrete on 28th day? why not on 27th day or 29th day? | LinkedIn <https://www.linkedin.com/pulse/why-do-we-test-concrete-28th-day-27th-29th-rajendran-c-eng-p-e/> (accessed Sep 7, 2020).

- (67) M.C. Miller Manufacturing - Trusted by Corrosion Engineers Worldwide - Miller 400D <https://www.mcmiller.com/miller-400d-44550> (accessed Sep 7, 2020).
- (68) Full Circle Squeeze Cellulose Sponge Absorbent Cloths 3-pack – Full Circle Home <https://fullcirclehome.com/products/squeeze> (accessed Sep 7, 2020).
- (69) Spragg, R. P.; De la Varga, I.; Montanari, L.; Graybeal, B. *Using Formation Factor to Define the Durability of Ultra-High Performance Concrete*; 2019.
- (70) CEMEX. The Effects of Water Additions to Concrete : “ What ’ s a Little Water Going to Hurt ?”. **2013**, 1–5.
- (71) Nindiyasari, F.; Griesshaber, E.; Zimmermann, T.; Manian, A. P.; Randow, C.; Zehbe, R.; Fernandez-Diaz, L.; Ziegler, A.; Fleck, C.; Schmahl, W. W. Characterization and Mechanical Properties Investigation of the Cellulose/Gypsum Composite. <https://doi.org/10.1177/0021998315580826>.
- (72) USG. Pottery Plaster, Submittal Sheet. **2005**, No. 1.
- (73) Clarkson, C. M.; El Awad Azrak, S. M.; Schueneman, G. T.; Snyder, J. F.; Youngblood, J. P. Crystallization Kinetics and Morphology of Small Concentrations of Cellulose Nanofibrils (CNFs) and Cellulose Nanocrystals (CNCs) Melt-Compounded into Poly(Lactic Acid) (PLA) with Plasticizer. *Polymer (Guildf)*. **2020**, *187*, 122101. <https://doi.org/10.1016/j.polymer.2019.122101>.
- (74) de Assis, C. A.; Iglesias, M. C.; Bilodeau, M.; Johnson, D.; Phillips, R.; Peresin, M. S.; Bilek, E. M. T.; Rojas, O. J.; Venditti, R.; Gonzalez, R. Cellulose Micro- and Nanofibrils (CMNF) Manufacturing - Financial and Risk Assessment. *Biofuels, Bioprod. Biorefining* **2018**, *12* (2), 251–264. <https://doi.org/10.1002/bbb.1835>.
- (75) Perejón, A.; Sánchez-Jiménez, P. E.; Criado, J. M.; Pérez-Maqueda, L. A. Kinetic Analysis of Complex Solid-State Reactions. A New Deconvolution Procedure. *J. Phys. Chem. B* **2011**, *115* (8), 1780–1791. <https://doi.org/10.1021/jp110895z>.
- (76) Gan, P. G.; Sam, S. T.; Abdullah, M. F. bin; Omar, M. F. Thermal Properties of

Nanocellulose-reinforced Composites: A Review. *J. Appl. Polym. Sci.* **2020**, *137* (11), 48544. <https://doi.org/10.1002/app.48544>.